HHS Public Access

Author manuscript

Nature. Author manuscript; available in PMC 2023 January 30.

Published in final edited form as:

Nature. 2022 May ; 605(7911): 736–740. doi:10.1038/s41586-022-04729-7.

Intracellular lipid surveillance by small G protein geranylgeranylation

Abigail Watterson[1], **Lexus Tatge**[1], **Naureen Wajahat**[1,2], **Sonja L. B. Arneaud**[1], **Rene Solano Fonseca**[1], **Shaghayegh T. Beheshti**[1,2], **Patrick Metang**[1], **Melina Mihelakis**[1], **Kielen R. Zuurbier**[1], **Chase D. Corley**[3,4], **Ishmael Dehghan**[1], **Jeffrey G. McDonald**[3,4], **Peter M. Douglas**[1,5]

[1]Department of Molecular Biology, University of Texas Southwestern Medical Center, Dallas, TX, USA.

[2]University of Texas at Dallas, Richardson, TX, USA.

[3]Center for Human Nutrition, University of Texas Southwestern Medical Center, Dallas, TX, USA.

[4]Department of Molecular Genetics, University of Texas Southwestern Medical Center, Dallas, TX, USA.

[5]Hamon Center for Regenerative Science and Medicine, University of Texas Southwestern Medical Center, Dallas, TX, USA.

Abstract

Imbalances in lipid homeostasis can have deleterious effects on health[1,2]. Yet how cells sense metabolic demand due to lipid depletion and respond by increasing nutrient absorption remains unclear. Here we describe a mechanism for intracellular lipid surveillance in *Caenorhabditis elegans* that involves transcriptional inactivation of the nuclear hormone receptor NHR-49 through its cytosolic sequestration to endocytic vesicles via geranylgeranyl conjugation to the small G protein RAB-11.1. Defective de novo isoprenoid synthesis caused by lipid depletion limits RAB-11.1 geranylgeranylation, which promotes nuclear translocation of NHR-49 and activation of *rab-11.2* transcription to enhance transporter residency at the plasma membrane. Thus, we identify a critical lipid sensed by the cell, its conjugated G protein, and the nuclear receptor whose dynamic interactions enable cells to sense metabolic demand due to lipid depletion and respond by increasing nutrient absorption and lipid metabolism.

peter.douglas@utsouthwestern.edu .

Author contributions

Conceptualization: A.W. and P.M.D. Methodology: A.W., L.T., N.W., S.L.B.A., R.S.F., I.D., C.D.C., J.G.M. and P.M.D. Investigation: A.W., L.T., N.W., S.L.B.A., R.S.F., S.T.B., P.M., M.M. and K.R.Z. Writing, review and editing: A.W., S.L.B.A. and P.M.D. Funding acquisition, resources and supervision: P.M.D.

Additional information

Supplementary information

The online version contains supplementary material available at https://doi.org/10.1038/s41586-022-04729-7.

Peer review information *Nature* thanks Peter Espenshade and the other, anonymous, reviewers for their contribution to the peer review of this work. Peer review reports are available.

Competing interests The authors declare no competing interests.

Defective lipid homeostasis negatively affects viability, yet organisms are highly refractory to these metabolic perturbations. Systemic lipid surveillance by hypothalamic neurons integrates signals from the intestine and elicits peripheral responses in hepatic cells through secreted endocrine factors that alter feeding behaviors as well as mobilize, utilize and store energy[1,2]. However, widespread cellular heterogeneity and differential access to systemic resources within a given tissue suggest that autonomous regulatory mechanisms of lipid homeostasis may have critical roles in health and disease. Although cells oscillate between catabolic and anabolic processes to adapt to their ever-changing environment, the vast diversity of lipid species presents a daunting task for the cell to sense the availability of thousands of these unique energy-rich molecules. As it houses the majority of the animal's lipid reserves, the *C. elegans* intestinal epithelium serves as its predominant metabolic tissue[3] and an excellent model for understanding the cellular response to lipid depletion.

The worm nuclear hormone receptor NHR-49, which shares sequence homology with mammalian hepatic nuclear factor 4 (HNF4), activates β-oxidation upon starvation[4,5]. Canonically, nuclear receptors are constitutively bound to chromosomal DNA, and ligand binding initiates polymerase recruitment and transcriptional activity[6]. However, in fed conditions, NHR-49::GFP decorated cytosolic vesicles marked by the lipophilic styryl dye, FM4–64 (Fig. 1a). Although a limited number of nuclear receptors are sequestered in the cytosol[7], none have been reported on endocytic vesicles. After starvation for 24 h, NHR-49::GFP shifted from cytosolic vesicles to the nucleus, accompanied by increased transcriptional activity, as indicated by increased fluorescence of its established transcriptional reporter, *acs-2p*::GFP[8] (Fig. 1b, c, Extended Data Fig. 1a–f). Gene ontology analysis of proteins immunoprecipitated with NHR-49::GFP identified a significant enrichment of interacting proteins involved in receptor-mediated endocytosis (Extended Data Fig. 1g). Furthermore, 58% (59 out of 101) of the annotated endocytosis-related proteins were enriched in NHR-49::GFP immunoprecipitations (Fig. 1d, Extended Data Table 1). Proteins associated with autophagic vesicles were not detected with NHR-49::GFP, highlighting its selective association with endocytic vesicles.

Rab GTPases serve as critical regulators of endocytic transport and subcellular trafficking of membrane proteins[9]. Given the link between nutrient availability and NHR-49 vesicular association, we investigated whether Rab GTPases influence this interaction. Similar to the shift in NHR-49::GFP localization, starvation also reduced Rab GTPase association with endocytic transport vesicles (Fig. 1e). RNA interference (RNAi) of individual Rab GTPases identified RAB-11.1 as the only GTPase tested whose knockdown promoted NHR-49::GFP nuclear accumulation and *acs-2p*::GFP activation (Fig. 1f, Extended Data Fig. 1h–j). Thus, RAB-11.1 affects the nucleocytoplasmic distribution and transcriptional activity of NHR-49.

To buffer starvation conditions, cells activate β-oxidation to mobilize intrinsic energy reserves and increase absorption to maximize uptake of the limited environmental resources[10–12]. However, starvation-induced dissociation of Rab GTPases from vesicles would negatively impact membrane trafficking and pose a problem for cellular absorption. Thus, we examined potential response factors activated upon *rab-11.1* RNAi that could restore Rab homeostasis, and identified the *rab-11.1* paralogue *rab-11.2* as the only transcriptionally activated Rab GTPase (Fig. 2a, Extended Data Fig. 2a, b). This 24-

fold activation presents an atypical mode of Rab GTPase regulation, which canonically occurs through post-translational means[9]. Generation of a *rab-11.2* transcriptional reporter, *rab-11.2p*::YFP, revealed its activation specifically in the intestine by *rab-11.1* RNAi as well as starvation (Fig. 2b, c, Extended Data Fig. 2c, d). We engineered a *rab-11.2(syb2999)* null mutation and observed no obvious phenotypes under permissive conditions (Fig. 2d, Extended Data Fig. 2e). However, the *rab-11.2(syb2999)* mutation hypersensitized worms treated with *rab-11.1* RNAi to starvation-induced toxicity (Fig. 2d), suggesting functional redundancy between the paralogues.

The Rab11 subfamily of GTPases regulates cell-surface residency of membrane proteins, including transporters required for nutrient absorption[13]. Although not apparent upon the onset of *rab-11.2* activation in larvae, *rab-11.1* RNAi markedly reduced the steady-state levels of the apically localized intestinal transporters PGP-3::mCherry and PEPT-1::DsRed by day 3 of adulthood, and this effect was further exacerbated in *rab-11.2(syb2999)* mutants (Fig. 2e, f, Extended Data Fig. 2f–i). Moreover, the *rab-11.2(syb2999)* mutation enhanced *rab-11.1* RNAi-mediated defects in intestinal absorption and lipid accumulation (Fig. 2g–j, Extended Data Fig. 2j–l). Preceding malabsorption, *rab-11.2* activation probably compensates for apical recycling defects caused by impairment of its constitutive paralogue RAB-11.1 in an effort to restore nutrient absorption and lipid homeostasis.

Starvation promoted the nuclear translocation and transcriptional activity of NHR-49, but the nature of the molecule(s) responsible for initiating these events was unclear. To identify this class of molecules, we disrupted energy homeostasis by reducing the expression of various enzymatic or transcriptional regulators involved in lipid metabolism, amino acid metabolism, glycolysis, ATP sensing, insulin signalling or age regulation. From this screen, lipid metabolism genes were the only set whose RNAi induced *rab-11.2p*::YFP activation (Fig. 3a, Extended Data Fig. 3a). Further investigation revealed that independently inhibiting fatty acid synthesis (*fasn-1* RNAi), fatty acid metabolism (*acs-1* RNAi), biosynthesis of unsaturated fatty acids (fat-6/7 RNAi), sphingolipid metabolism (sptl-1 RNAi), glycerophospholipid metabolism (lpin-1 RNAi), sterol metabolism (sbp-1 RNAi) or prenol synthesis (hmgr-1 RNAi) activated rab-11.2p::YFP fluorescence in all conditions (Fig. 3a, b, Extended Data Fig. 3a, b). This suggests that rab-11.2 is activated in response to various types of lipid depletion.

To examine how lipid depletion affects the nucleocytoplasmic dynamics of NHR-49, we impaired fatty acid metabolism through RNAi of the acyl-coenzyme A (acyl-CoA) synthetase ACS-1, which catalyzes the cytosolic conversion of free fatty acids to acyl-CoA[14]. Loss of lipid accumulation by acs-1 RNAi corresponded with Rab GTPase dissociation from vesicles and reduced cell-surface residency of apical intestinal transporters (Extended Data Fig. 3c–i). These metabolic and physiological changes initiated by acs-1 RNAi were accompanied by the nuclear accumulation and increased activity of NHR-49 (Fig. 3c, Extended Data Fig. 3j–l). Furthermore, increased rab-11.2p::YFP fluorescence caused by acs-1 RNAi was abolished in nhr-49(nr2041) loss-of-function mutants[4] (Fig. 3d, Extended Data Fig. 3m). Conversely, baseline rab-11.2::YFP fluorescence was increased in nhr-49(et13) gain-of-function mutants[15] (Extended Data Fig. 3n). Thus, limited lipid

availability elicits a transcriptional response through NHR-49, including activation of rab-11.2.

Despite the vast diversity of lipids, we proposed that cells monitor their global lipid availability by sensing a particular lipid species that is synthesized de novo rather than ingested. Upon digestion and absorption, complex molecules are catabolized into simpler 'building blocks' that can be reinvested into different biosynthetic pathways to accommodate cellular needs[10,16]. Dietary lipids are broken down to acyl-CoA, which is imported into mitochondria via the carnitine system and undergoes β-oxidation to generate acetyl-CoA and NADH as respiratory substrates[17]. Acetyl-CoA can alternatively be exported from mitochondria as citrate and converted back to acetyl-CoA in the cytosol for purposes of de novo lipid synthesis or protein acetylation[17]. RNAi knockdown of the carnitine acyltransferase importers *cpt-2* and *cpt-3* or the citrate exporter *K11H3.3* was sufficient to activate *rab-11.2p*::YFP fluorescence (Extended Data Fig. 4a, b). In support of the putative sensor being synthesized de novo, reduced acetyl-CoA flux through mitochondria promotes pathway activation.

Conditions that reduce global fat accumulation might indirectly affect levels of the particular lipid sensed by the cell. Whereas impairment of six of the seven lipid metabolic pathways examined reduced lipid levels, RNAi of the rate-limiting hydroxymethylglutaryl-CoA (HMG-CoA) reductase enzyme[18] (*hmgr-1*) in the isoprenoid pathway (also known as the mevalonate pathway) was the only condition that did not affect overall lipid levels upon the onset of *rab-11.2* activation in day 1 adult worms (Extended Data Fig. 4c). Since this biosynthetic pathway produces the lipid moiety required for Rab GTPase vesicular association[19,20], we hypothesized that the isoprenoid pathway synthesizes the critical lipid by which cells sense lipid availability, and that its selective impairment activates the lipid surveillance response even without global lipid loss. In this pathway, cytosolic acetyl-CoA is converted into the five-carbon isopentenyl pyrophosphate, which serves as the precursor for every sterol and prenol lipid[18,21]. In particular, the polyunsaturated 15-carbon farnesyl and 20-carbon geranylgeranyl pyrophosphates are covalently linked to cysteines within the C-terminus of most every small G protein, serving as membrane anchors[22]. Conjugation of these lipid moieties to small G proteins requires prenyltransferase holoenzymes; the type II geranylgeranyltransferase exclusively modifies Rab GTPases, whereas the farnesyltransferase and type I geranylgeranyltransferase modify all other small G proteins[19,20] (Fig. 4a). RNAi knockdown of enzymes upstream of prenol synthesis activated *rab-11.2p*::YFP fluorescence (Fig. 4a, b, Extended Data Fig. 4d). Furthermore, RNAi knockdown of the type II geranylgeranyltransferase subunits, but not the type I or farnesyltransferase subunits, was sufficient for reporter activation (Fig. 4a, b, Extended Data Fig. 4d). Thus, geranylgeranyl synthesis and conjugation to Rab GTPases have important roles in pathway regulation. Moreover, transcriptomics in worms hinted at the importance of the type II transferase due to selective activation of its subunits upon *rab-11.1* RNAi (Extended Data Fig. 4e). This response appears to be conserved, as evidenced by the mevalonate-dependent activation of the *rab-11.2* homologue *RAB11A* in primary human endothelial cells by pharmacological inhibition of HMG-CoA reductase[23] (Extended Data Fig. 4f).

To further investigate the role of geranylgeranyl synthesis and transfer in lipid surveillance, we focused on the rate-limiting enzyme HMGR-1 and the downstream type II geranylgeranyl transferase β-subunit GGTB-1. Examination of GFP::RAB-11.1 confirmed its impaired association with vesicles in *hmgr-1* and *ggtb-1* RNAi conditions (Extended Data Fig. 5a). This loss of Rab GTPase vesicular adaptation elicited a loss of apical transporter levels, impaired intestinal absorption, and reduced lipid deposition by day 3 of adulthood (Extended Data Fig. 5b–h). Preceding these defects, both *hmgr-1* and *ggtb-1* RNAi promoted NHR-49 nuclear translocation and transcriptional activity in day 1 adult worms, including activation of *acs-2p*::GFP as well as *rab-11.2p*::YFP in an NHR-49-dependent fashion (Fig. 4c, Extended Data Fig. 4h–l). Thus, defective Rab geranylgeranylation activates this adaptive response through NHR-49 nuclear translocation.

To determine whether geranylgeranyl pyrophosphate is a critical determinant in lipid sensing, we investigated whether its levels become depleted at the time of pathway activation. Without any detectable loss in acetyl-CoA levels, targeted lipidomics revealed 70–90% reductions in geranylgeranyl levels after starvation or upon inhibition of either fatty acid or isoprenoid synthesis (Fig. 4d). Depletion of geranylgeranyl pyrophosphate synthesis by *hmgr-1* RNAi corresponded to 34–54% losses in geranylgeranylation of the Rab GTPases examined (Fig. 4e, Extended Data Fig. 5i–k). Similarly, impaired fatty acid synthesis via *acs-1* RNAi reduced GFP::RAB-11.1 geranylgeranylation by 29% (Fig. 4e, Extended Data Fig. 5k). To further examine whether geranylgeranyl serves as the critical lipid in this pathway, we restored geranylgeranyl levels by media supplementation with the alcohol derivative geranylgeraniol. Geranylgeraniol addition increased levels of geranylgeranylated GFP::RAB-11.1 upon *acs-1* and *hmgr-1* RNAi (Fig. 4e, Extended Data Fig. 5k). Furthermore, geranylgeraniol supplementation reduced or even abrogated defects in GFP::RAB-11.1 vesicular association, apical transporter residency, cellular absorption and lipid accumulation caused by *hmgr-1* and *acs-1* RNAi in day 3 adults (Extended Data Fig. 5). Importantly, restoration of Rab geranylgeranylation was sufficient to rescue NHR-49::GFP cytosolic sequestration and prevent *rab-11.2p*::YFP activation upon *hmgr-1* and *acs-1* RNAi (Fig. 4f, g, Extended Data Fig. 6a–h). This appears to be specific for geranylgeranyl, as supplementation with the sterol precursor squalene or the monounsaturated fatty acid oleic acid did not prevent NHR-49 nuclear accumulation and transcriptional activity (Extended Data Fig. 6a–c). While restoration of geranylgeranyl availability attenuated pathway activation in *hmgr-1* and *acs-1* RNAi conditions, geranylgeraniol supplementation did not prevent its activation by *ggtb-1* RNAi, nor did it rescue RAB-11.1 vesicular association or the ensuing absorptive and lipid accumulation defects caused by *ggtb-1* RNAi (Fig. 4f, g, Extended Data Fig. 6a–d). Despite the presence of geranylgeraniol, these data suggest that its conjugation to Rab GTPases by the geranylgeranyl transferase is required for NHR-49 vesicular sequestration and inactivation. There fore, pathway activity is dependent on geranylgeranyl availability and conjugation to Rab GTPases.

Having demonstrated the importance of RAB-11.1 in the nucleocyto-plasmic dynamics of NHR-49 (Fig. 1), we sought to determine whether RAB-11.1 might represent the critical substrate for geranylgeranylation. Despite geranylgeraniol addition, NHR-49::GFP remained nuclear and transcriptionally active with *rab-11.1* RNAi (Fig. 4h, i, Extended Data Fig. 6i, j).

To further investigate the necessity of RAB-11.1 geranylgeranylation for NHR-49 vesicular sequestration, we generated transgenic worms expressing mRuby2-tagged RAB-11.1 or RAB-11.1(C208A/ C209A), which has point mutations in its C-terminal di-cysteine motif to prevent geranylgeranyl conjugation (Extended Data Fig. 6k, l). In parallel, we engineered an alternate *rab-11.1* RNAi construct targeting the 3′ untranslated region (UTR) of endogenous *rab-11.1* transcripts, enabling selective knockdown of endogenous *rab-11.1* while retaining expression of ectopic mRuby2::RAB-11.1. We confirmed that *rab-11.1* 3′ UTR RNAi promoted the nuclear translocation of NHR-49::GFP, and ectopically rescuing *rab-11.1* expression with mRuby2::RAB-11.1 was sufficient to retain NHR-49::GFP in the cytosol (Fig. 4j). Expression of the mRuby2::RAB-11.1(C208A/C209A) geranylgeranyl motif mutant, however, was unable to retain NHR-49::GFP in the cytosol (Fig. 4j). Therefore, RAB-11.1 geranylgeranylation directly affects the nucleocytoplasmic dynamics of NHR-49 and is required to suppress activation of the intracellular lipid surveillance pathway.

Cells buffer unfavourable environmental and intrinsic conditions through a wide range of adaptive responses. Utilization of intrinsic energy reserves in de novo synthesis pathways compensates for lipid deficits upon starvation, but eventual resource exhaustion limits the cellular capacity to replenish necessary lipid molecules. We propose that cells sense global lipid availability by monitoring their capacity to synthesize the prenol lipid geranylgeranyl pyrophosphate through its enzymatic conjugation to the small G protein RAB-11.1. This post-translational modification of RAB-11.1 is required to sequester the nuclear hormone receptor NHR-49 to endocytic transport vesicles in conditions of ample resources, although the nature of this interaction remains undefined. Decreases in lipid availability reduce geranylgeranyl synthesis, and the subsequent depletion of geranylgeranylated RAB-11.1 prevents NHR-49 association with endocytic vesicles and promotes its nuclear translocation (Extended Data Fig. 7). Yet the question of how cells establish the threshold for RAB-11.1 geranylgeranylation in lipid surveillance and how this relates to other lipidated proteins remains open. In the nucleus, NHR-49 regulates the expression of target genes that control the uptake and utilization of dietary lipids. It also remains unclear how *rab-11.2* activation compensates for reduced RAB-11.1 functionality when geranylgeranyl levels are limited. Nonetheless, this proposed pathway links the cell's ability to sense metabolizable lipid availability with cellular absorption through orchestration of cell-surface residency of membrane proteins by the Rab11 subfamily of GTPases. In summary, this simple yet elegant lipid surveillance mechanism provides a means for cells to monitor and respond to a broad spectrum of catabolic and anabolic defects. Rather than sensing thousands of distinct lipid species, cells appear to be capable of surveying an infinitely heterogeneous pool of lipids by monitoring their breakdown to acetyl-CoA and its subsequent synthesis into geranylgeranyl pyrophosphate.

Online content

Any methods, additional references, Nature Research reporting summaries, source data, extended data, supplementary information, acknowledgements, peer review information; details of author contributions and competing interests; and statements of data and code availability are available at https://doi.org/10.1038/s41586–022-04729–7.

Methods

C. elegans strains and maintenance

All strains were maintained on an OP50 *Escherichia coli* lawn grown on standard NGM plates. For experimental purposes, worm strains were grown on NGM plates supplemented with HT115 *E. coli* at 20 °C unless otherwise noted. Age synchronization was performed by hypochlorite treatment of gravid animals to obtain eggs. AGP33a (*glmEx8(nhr-49p::nhr-49::gfp + myo3p::mCherry); nhr-49(nr2041) I*) worms were obtained from the laboratory of A. Ghazi[5]. MZE1 (*unc-119(ed3) III; cbgIs91[pept-1p::pept-1::DsRed + unc-119(+)]; rrf-3(pk1426) II; pwls69[vha-6p::gfp::rab-11 + unc-119(+)]*) worms were obtained from the laboratory of M. Zerial[24]. The following strains were obtained from Caenorhabditis Genetics Center: N2 (*ancestral wild-type*), CF512 (*rrf-3(b26) II; fem-1(hc17) IV*), STE68 (*nhr-49(nr2041) I*), LIU1 (*ldrIs1[dhs-3p::dhs-3::gfp + unc-76(+)]*), WBM170 (*wbmEx57[acs-2p::gfp + rol-6(su1006)]*), VK2734 (*vkIs2734[nhx-2p:: lmn-1::CemOrange2 + myo-2p::gfp]*), RT327 (*pwIs72[vha-6p::gfp::rab-5 + Cbr-unc-119(+)] II*), RT476 (*pwIs170[vha6p::gfp::rab-7 + Cbr-unc-119(+)]*), RT525 (*pwIs206[vha6p::gfp::rab-10 + Cbr-unc-119(+)]*), RT311 (*pwls69[vha-6p::gfp::rab-11.1 + unc-119(+)]*), OG472 (*drSi2 [vha-6p::3xflag::pgp-3/CFTR(wt)::mCherry] II*), and QC126 (*nhr-49(et13) I; paqr-2(tm3410) III*).

The following strains were produced for this study: PHX2999 (*rab-11.2(syb2999) I*) was generated by SunyBiotech and includes a 731 base pair deletion encompassing the entire length of the *rab-11.2* gene. Gene knockout was PCR and sequence validated. PHX4435 (*rab-11.1(syb4435[gfp::rab-11.1] I)*) was generated by SunyBiotech and includes an insertion of *gfp* directly upstream of the endogenous *rab-11.1* gene locus. PMD104 (*utsEx14[rab-11.2p::yfp]*) was made by microinjection into N2, PMD118 (*utsEx14[rab-11.2p::yfp]; nhr-49(nr2041) I*) by crossing PMD104 to STE68, PMD124 (*utsIs3[rab-11.2p::yfp]*) by integrating the extrachromosomal array into the genome via UV irradiation with three subsequent back-crosses to N2, PMD90 (*fem-1(hc17ts) IV; pwls209[vha-6p::gfp::rab-11.1 + Cbr-unc-119(+)]*) by crossing RT525 to CF512, PMD91 (*fem-1(hc17ts) IV; pwls69[vha-6p::gfp::rab-10 + Cbr-unc-119(+)]*) by crossing RT311 to CF512, PMD125 (*glmEx8[nhr-49p::nhr-49::gfp + myo2p::mCherry]; vkIs2734[nhx-2p::lmn-1::CemOrange2 + myo-2p::gfp]*) by crossing AGP33a to VK2743, PMD150 (*utsIs4[glmEx8(nhr-49p::nhr-49::GFP + myo3p::mCherry]; nhr-49(nr2041) I*) by integrating the APG33a transgenic construct into the genome via UV irradiation and backcrossing to N2, PMD169 (*cbgIs91[pept-1p::pept-1::DsRed + unc-119(+)]; rrf-3(pk1426) II; rab-11.2(syb2999) I*) by crossing MZE1 to PHX2999, PMD170 (*ldrIs1[dhs-3p::dhs-3::gfp + unc-76(+)]; rab-11.2(syb2999) I*) by crossing LIU1 to PHX2999, PMD204 (*utsEx31[pept-1p::mRuby2:: rab-11.1]*) and PMD205 (*utsEx32[pept-1p::mRuby2::rab-11.1(C208A,C2 09A)]*) by microinjection into N2, PMD208 (*utsEx31[pept-1p::mRuby2: :rab-11.1]; utsIs4[nhr-49p::nhr-49::GFP + myo-3p::mCherry]*) by crossing PMD204 to PMD150, PMD209 (*utsEx32[pept-1p::mRuby2::rab-11.1(C208 A,C209A)]; utsIs4[nhr-49p::nhr-49::GFP + myo-3p::mCherry]*) by crossing PMD205 to PMD150, and PMD212 (*utsIs3[rab-11.2p::yfp]*) and PMD213 (*utsEx39[nhr-49(et13) I; paqr-2(tm3410) III]; utsIs3[rab-11.2p::yfp]*) by

crossing QC126 to PMD124. PMD19 (*jyIs13×3[gfp::act-5] II; fer-15(b26) II; fem-1(hc17ts) IV*) was made as described[25]. See Supplementary Table 2 for strains used throughout this study.

Single worm genotyping

To identify worms carrying the *rab-11.2(syb2999)* and *nhr-49(nr2041)* deletion or *nhr-49(et13)* gain-of-function mutations, individual worms from the F_2 generation of genetic crosses were transferred to NGM plates seeded with OP50 and allowed to lay eggs. The F_2 adult worms were then frozen in 10 µl of worm genotyping lysis buffer (10 mM Tris-Base (pH 8.2), 50 mM KCl, 2.5 mM $MgCl_2$, 0.45% Tween-20, and 60 µg ml^{-1} Proteinase K (VWR), added immediately before use), for at least 15 min at −80 °C. Worms were lysed for 1 h at 60 °C, followed by proteinase K inactivation for 15 min at 95 °C. A standard PCR reaction was performed using primers for DNA immediately upstream and downstream of the respective mutation, listed in Supplementary Table 3. To identify worms carrying the *rab-11.2(syb2999)* and *nhr-49(nr2041)* mutations, PCR products were loaded onto a 1.0% agarose/TBE gel and electrophoresis was performed at 100 V for 1 h. Mutants were identified according to PCR product size (986 bp (*rab-11.2* wild-type) vs 230 bp (*rab-11.2(syb2999)*) and 1,000 bp (*nhr-49* wild-type) vs 100 bp (*nhr-49(nr2041)*)). To identify worms carrying the *nhr-49(et13)* T/A missense mutation, PCR products were incubated with the Hpy188III restriction enzyme (New England Biolabs R0622S) for 6 h at 37 °C prior to gel electrophoresis on a 1.0% agarose/TBE gel at 100 V for 1 h. The respective T/A missense mutation introduced a Hpy188III restriction enzyme cut site, resulting in cleavage of the PCR product.

Molecular cloning

Plasmids generated for this study were assembled using standard New England Biolabs (NEB) restriction enzyme digest and ligation protocols and transformed into DH5α cells. Mutations were generated using the Agilent QuikChange Lightning Site-Directed Mutagenesis kit (Fisher-Scientific NC9620881). All constructs were cloned into the plasmid vector pNB13 (provided by A. Dillin), which contains the *yfp* and *unc-54* 3′ UTR in pAD12 vector backbone (Addgene). Promoter regions (2 kb upstream of the *rab-11.2* or *pept-1* coding sequences) were cloned from *C. elegans* genomic DNA. *Rab-11.1* cDNA was synthesized by Genewiz. The mRuby2 sequence was provided by K. Dean. Primers containing 5′ and 3′ restriction enzyme sites were used to amplify fragments using TopTaq 2× Master Mix (Qiagen) and PCR settings: initial denaturing 95 °C, 30 s (hot start), 95 °C for 10 s, 54–72 °C annealing for 30–120 s, and 72 °C extension for 120 s, repeated for 35 cycles. Following PCR, products and plasmid vectors were digested with restriction enzymes (NEB) (XbaI/XmaI for *rab-11.2* promoter region, SphI/SalI for *pept-1* promoter region, XbaI/BamHI for *mRuby2*, and BamHI/EcoRI for *rab-11.1* cDNA) at 37 °C for at least 2 h, and then subject to heat inactivation at 65 °C for 15 min. Digested products were loaded onto a 1.0% agarose/TBE gel and electrophoresis was performed at 90 V for 1 h. Bands of interest were excised and purified using a Zymoclean Gel DNA Recovery Kit (Zymo Research) following the manufacturer's instructions. Concentration of gel-purified DNA was measured with a DeNovix DS-11 FX+, and ligation reactions (3:1 insert:vector ratio) were prepared accordingly. Following 1 h ligation with T4 DNA Ligase (NEB) at

room temperature and 10 min heat inactivation at 65 °C, DNA was transformed into DH5α cells via heat shock at 42 °C for 45 s, followed by incubation for 2 min on ice and 1 h at 37 °C in LB on an Eppendorf Thermomixer C shaker set to 300 rpm. Transformed bacteria were spread onto LB/Carbenicillin plates and incubated at 37 °C overnight. DNA was isolated from resulting colonies using the Monarch Plasmid Miniprep Kit (NEB) and sequenced to verify insertion of the respective DNA. The *rab-11.1(C208A,C209A)* mutation was generated using the Agilent QuikChange Lightning Site-Directed Mutagenesis kit according to manufacturer instructions. Primers were designed using the Agilent QuikChange Primer Design Program and are listed in Supplementary Table 3.

Regarding generation of RNAi constructs, nucleotide fragments were amplified from *C. elegans* cDNA and cloned into the pL4440 plasmid between the 5′ KpnI and either 3′ XhoI or HindIII restriction sites. A 385 base pair nucleotide fragment beginning 23 nucleotides downstream of the *rab-11.1* TAA stop codon was used to generate *rab-11.1 3'UTR* RNAi, and *fdps-1* RNAi was generated using 1,050 or 800 base pair nucleotide fragments. Primers are listed in Supplementary Table 3.

Worm microinjections

Worm microinjections were performed as described[26]. In brief, worms were injected using a FemtoJet 4i (Eppendorf) attached to a Leica DMi8 inverted stereomicroscope (Leica) using 0.78 mm inner diameter, 1.0 mm outer diameter pulled glass capillaries. Solutions containing 200 ng μl^{-1} (PMD104) or 75 ng μl^{-1} (PMD204 and PMD205) of plasmid in molecular biology grade water were injected into the gonad of day 1 adult N2 worms. The animals were then suspended in M9 buffer and recovered on a fresh lawn of OP50.

Integration of extrachromosomal arrays

Integration of transgenic constructs were performed using UV irradiation. Transgenic L4 larvae were irradiated in a UV cross-linker at 0.4 J cm^{-2} and recovered at 20 °C on OP50. Progeny expressing the transgenic marker (100–200 worms) were transferred to individual NGM plates seeded with OP50, and fully penetrant lines were maintained and back-crossed to N2 at least three times.

RNAi administration

Interfering RNAs were obtained from either the Vidal or Ahringer RNAi libraries, if available, or were generated for this study. All RNAi experiments were performed using HT115 *E. coli* containing either L4440 empty vector (EV) or various RNAi constructs. Liquid cultures of RNAi were grown in Terrific Broth (TB) for 14 h at 37 °C and then induced with 1 mM IPTG for 4 h at 37 °C. Cultures were concentrated to 1/10 of the original volume via centrifugation at 3,000*g* for 10 min, seeded onto RNAi plates (60 mm or 100 mm, containing 0.1 mg ml^{-1} carbenicillin and 1 mM IPTG, added 24 h prior to seeding), and allowed to dry for 1–2 days at room temperature, protected from light. Refer to Supplementary Table 3 for RNAi oligonucleotides.

Media supplementation

GGOH (Sigma-Aldrich G3278), oleic acid (Fisher Scientific 50–179-1580), and squalene (Sigma-Aldrich S3626) were diluted in molecular biology grade water to 100 mM stock solutions (stored at −20 °C). Solutions were thawed to room temperature, incubated at 37 °C for 15 min, and vortexed for 1 min prior to media supplementation. Plates seeded with HT115 *E. coli* were supplemented with 1 mM GGOH, oleic acid, or squalene and allowed to dry for 24 h in the dark prior to age synchronization. Equivalent volumes of molecular biology grade water were added to control plates.

Oil-red-O staining

To assess major fat stores, worms were fixed and stained with 60% oil-red-O isopropanol solution. For each condition, 200–300 worms were rinsed off plates with M9 buffer, centrifuged (1,000*g*) for 30 s in a room temperature clinical centrifuge, suspended in 1 ml 1× PBS in 1.5 ml Eppendorf tubes, and washed three times in 1× PBS via centrifugation (1,000*g*) for 10 s. To permeabilize the cuticle, worms were suspended in 2× MRWB (3.7% formaldehyde, 160 mM KCl, 40 mM NaCl, 14 mM EDTA, 0.2 % β-mercaptoethanol) diluted to 1× in PBS and incubated while rocking for 1 h at room temperature. Following three washes with 1× PBS, worms were incubated while rocking in 60% isopropanol for 15 min and then stained with 60% oil-red-O for 18 h (note: prior to the experiment, 0.5 g per 100 ml oil-red-O isopropanol stock solution (Fisher Scientific AAA1298914) was rocked for 3–4 days, diluted with 40% MilliQ water, filtered through a 0.45-μm filter, and rocked overnight). Following staining, dye was removed and replaced with 1× PBS + 0.01% Triton-X. Worms were rocked for 2 min and then washed twice with 1× PBS. Worms were then mounted on a 1% agarose pad for imaging.

TRITC–BSA and FM4–64 absorption assays

To assess endocytosis efficiency across the apical surface of the intestine, approximately 100 adult worms were rinsed off plates with M9 buffer, washed twice with fresh M9 via centrifugation (1,000*g*) for 30 s, and incubated in 50 μl of TRITC–BSA (1 mg ml^{-1}) (Fisher Scientific A23016) in M9 buffer or FM4–64 (0.4 mM) (Fisher Scientific T3166) in FM4–64 buffer[27]. Samples were incubated in an Eppendorf Thermomixer C shaker set to 300 rpm for 2 h at 20 °C. Worms were washed three times with M9 buffer, then allowed to recover on NGM plates seeded with OP50 for 2 h in the dark. For quantification of endocytosis efficiency, worms were visualized under an Axio Observer inverted microscope (Carl Zeiss Microscopy) at 50× magnification and scored according to the three absorption efficiency categories demonstrated in Extended Data Fig. 2j. For imaging purposes, worms were rinsed off plates with M9 buffer, centrifuged (1,000*g*) for 30 s, and mounted on slides in M9 supplemented with 100 mM levamisole.

Starvation assays

For 24 h starvation experiments, age-synchronized worms were grown on EV RNAi until larval stage L4. Worms were rinsed off plates with M9 buffer, washed twice with fresh M9 via centrifugation (1,000*g*) for 30 s, and then transferred via glass pipette to RNAi

(NGM/carbenicillin/IPTG) plates without food (starvation conditions) or supplemented with EV RNAi (ad libitum-fed control) for 24 h.

For starvation-induced toxicity assays, age-synchronized animals were treated with RNAi until larval stage L4. Worms were then transferred to empty NGM/carbenicillin plates for 24 h. Following dietary deprivation, worms were rinsed off plates with liquid M9 buffer, washed twice with fresh M9 buffer via centrifugation (1,000*g*) for 30 s, and then incubated in 1 μg ml^{-1} propidium iodide for 10 min with agitation, protected from light. The propidium iodide solution was then aspirated and the worms were washed one additional time with M9 buffer, centrifuged (1,000*g*) for 1 min, and analysed by large-particle flow cytometry.

Nuclear NHR-49::GFP quantification

Age-synchronized transgenic worms expressing NHR-49::GFP were visualized under an Axio Observer inverted microscope (Carl Zeiss Microscopy) at 100× magnification. Observers were blinded to sample condition by randomly assigning letters to the plates prior to visualization. The number of fluorescent intestinal nuclei were counted for each individual worm (at least 15 worms per condition for each biological replicate); NHR-49::GFP was considered nuclear if the fluorescence intensity in the nucleus exceeded that of the cytosolic signal proximal to the nucleus by at least twofold. Percentage was calculated by dividing the respective number of NHR-49::GFP-positive nuclei by 20 (number of intestinal cells in *C. elegans*). Percentage distributions for each condition were analysed using Prism 9 software (ver. 9.0, GraphPad).

Microscopy

For fluorescence micrographs of transcriptional reporter strains, 6 worms per condition were aligned on NGM/carbenicillin plates in a drop of M9 supplemented with 100 mM levamisole. Imaging was performed on a Zeiss Axio Observer inverted microscope using a Zeiss 20× Plan-Apochromat air immersion objective (0.8 NA, 0.55 mm WD) set to 80× magnification. Images were acquired using transmitted light and standard filter settings for excitation and emission of fluorescence probes and recorded on a CCD camera (Zeiss AxioCam MRm). Zeiss ZEN software (blue edition) was used to control acquisition. Exposure settings and additional processing parameters remained consistent among samples in each experiment. Oil-red-O staining was observed using a Zeiss Axio Observer Z1 inverted microscope with an MRC-Color camera. Zeiss ZEN software was used to control acquisition. Confocal micrographs were acquired using a Leica SP8 confocal microscope (Leica) and Leica Application Suite X (LAS X) software (ver. 3.5.5). Staining for DAPI on formaldehyde-fixed, permeabilized worms was performed as previously described[25]. For all other confocal imaging, live worms were mounted in M9 supplemented with 100 mM levamisole and samples were imaged at 40× or 63× with oil immersion. All images were acquired in *xyz* acquisition mode, and each line was imaged three times and averaged to reduce noise. Lasers 488 and/or 552 were used to excite fluorophores using hybrid detectors. Laser power, range and gain were adjusted according to strain/experiment but remained consistent between trials.

Large-particle flow cytometry

Age-synchronized worms were analysed by flow cytometry through use of a COPAS FP-250 flow cytometer (Union Biometrica). Worms were acquired using the attached sample cup or from a 96-well plate by an LP Sampler. Sample solution was comprised of M9, and flow sheath solution contained the COPAS GP Sheath Reagent (PN: 300–5070-100, Union Biometrica) proprietary recipe. Flow data was collected and processed using the FlowPilot software (ver. 2.6.1, Union Biometrica). Further data processing was performed in Excel (Microsoft) and statistical analysis in Prism 9 (Graphpad). Extinction was detected using the 488 nm laser line with a 1.3 ND filter and gain of 1.0. Propidium iodide, mCherry and DsRed were excited using a 561 nm laser, while YFP and GFP were excited using a 488 nm laser. Gains for fluorescence detection were set to 2.0, and PMT voltage adjusted within the linear range of the instrument was consistent for each experiment (500 for YFP, mCherry, DsRed and 450 for GFP). Peak fluorescence intensity values from individual worms (standardized relative to EV RNAi control) were used for dot plots. Otherwise, the integral of the fluorescence intensity for each worm within samples was averaged, and mean values were normalized according to time-of-flight to account for variation in worm size across RNAi conditions. Normalized mean fluorescence values were standardized relative to EV RNAi control. Reference Supplementary Fig. 2 for gating strategy.

Proteomics sample preparation and LC–MS/MS measurement

Age-synchronized non-transgenic (N2) and transgenic (PMD150) worms expressing NHR-49::GFP were cultured on RNAi (NGM/carbenicillin/ IPTG) plates supplemented with EV RNAi. Worms were allowed to develop until late larval stage L4 and then washed off the plates with M9 buffer, centrifuged (1,000*g*) for 30 s, and washed twice with M9 liquid buffer before being transferred to 1.5 ml Eppendorf tubes and rapidly flash frozen in liquid nitrogen. Worm extracts were generated by glass bead disruption in non-denaturing lysis buffer (50 mM Hepes pH 7.4, 150 mM NaCl, 1mM EDTA, 1% Triton X-100, EDTA-free mini-protease inhibitor cocktail (Roche)). Crude lysates were subject to centrifugation at 8,000*g* at 4 °C for 5 min. For co-immunoprecipitation, pre-cleared worm extracts were first supplemented with 5 μl (2 μg) of mouse anti-GFP monoclonal antibody (Roche 11814460001) and incubated for 1 h. Next, 100 μl of SureBeads Protein G magnetic beads (Bio-Rad 1614013) were added, and the lysate–antibody mix was rotated 360 degrees for 1 h at 4 °C. Following incubation, the G-protein beads were magnetically precipitated and gently washed 3 separate times with 1 ml of non-denaturing lysis buffer before being resuspended in 30 mM Triethylammonium bicarbonate (TEAB) buffer containing 4% SDS for sample elution.

To prepare samples for LC–MS/MS analysis, disulfide bonds were reduced with 20 mM DTT, followed by alkylation with 40 mM iodoacetamide and acidification by phosphoric acid. Samples were diluted in binding buffer (1 to 9 volume of TEAB to methanol) and loaded onto S-Trap micro columns (Protifi). Proteins were digested with a ratio of 1:25 trypsin (Pierce) overnight at 37 °C, and eluted peptides were dried out in a speedvac and reconstituted in 2% acetonitrile and 0.1% trifluoroacetic acid. Peptides were separated using an UltiMate 3000 RSLC nano LC system (Thermo Fisher Scientific) equipped with an EASY-Spray 150 mm column with a 75 μM inner diameter (Thermo Scientific ES800A)

heated at 55 °C. Gradient elution was performed from 2% acetonitrile to 30% acetonitrile in 0.1% formic acid over 90 min. Q-Exactive HF mass spectrometer was set to acquire data in data-dependent top 20 method with the full-MS scans acquired at 120K resolution and MS/MS scans acquired at 15K resolution (at *m/z* 200). Normalized collision energy was 28 and the minimum AGC trigger was 2×10^2 ions (intensity threshold 1×10^3). The peptide match algorithm was set to preferred and charge exclusion was applied to exclude unassigned peptides. Dynamic exclusion and charge 1 and > 8 species were applied with a duration of 20 s.

Proteomics searches were performed using the *C. elegans* reference database from UniProt with Proteome Discoverer 2.4. Peptides with a minimum of six amino acid residues with trypsin/P specificity were identified. Protein N-terminal acetylation and carbamidomethyl of cysteine were used as fixed modifications, and methionine oxidation was used as a variable modification. Proteins were considered enriched if detected in at least two biological replicates, enriched at least 1.5-fold over non-transgenic control, and peptide spectral match (PSM) ≥ 2. Reference Supplementary Data 1 for complete dataset.

Gene Ontology analysis

DAVID Bioinformatics Resources[28,29] 6.8 (https://david.ncifcrf.gov/) was used for Gene Ontology and KEGG pathway analysis of proteins enriched in NHR-49::GFP immunoprecipitations. Proteins analysed by DAVID met the following criteria: (1) a minimum of two signals were detected from the 3 biological replicates; (2) PSM ≥ 2; (3) average signal from the 3 biological replicates was enriched at least 1.5-fold over the non-transgenic immunoprecipitation control. Enrichment score was calculated from the false discovery rate (FDR).

Illumina RNA sequencing and transcriptomic analysis

Three biological repeats of age-synchronized wild-type L4 larvae cultured on EV or *rab-11.1* RNAi were collected and rapidly flash frozen in liquid nitrogen. RNA was purified by chloroform/phenol extraction followed by isopropanol precipitation and two washes with 75% ethanol before resuspension in 50 µl molecular biology grade water. Quality control, mRNA purification, and paired-end 150 bp Illumina sequencing was performed by Novogene as previously described[26]. Statistical analysis was performed using CLC Genomics Workbench software (ver. 9.5, Qiagen Bioinformatics). Gene expression data were compared by Baggerly's test with FDR correction. Genes were considered significantly regulated by *rab-11.1* RNAi when absolute fold change ≥ 2 and p-value < 0.05. Phenotype enrichment analysis of the genes differentially regulated by *rab-11.1* RNAi was performed using the Wormbase Enrichment Analysis resource (wormbase.org/tools/enrichment/tea/tea.cgi)[30].

Transcriptomic analysis of human microvascular endothelial cells[23] treated with or without atorvastatin or atorvastatin and mevalonate was acquired from Gene Expression Omnibus (GEO) (accession GSE8686). Rab GTPase transcript abundance values were standardized relative to vehicle control. Rabs were omitted from analysis if detected in fewer than 3

replicates for any condition. Prism 9 (GraphPad) was used for heatmap generation and statistical analysis. See Supplementary Table 1 for statistical results.

Geranylgeranyl measurement by mass spectrometry

Age-synchronized CF512 worms were cultured at 25 °C until day 1 of adulthood. For starvation conditions, worms were removed from food 24 h prior to sample collection. Worms were rinsed off plates and washed three times with liquid M9 buffer by centrifugation (1,000*g*) for 30 s. In equal volumes, worm pellets were transferred to 1.5 ml Eppendorf tubes and samples were flash frozen in liquid nitrogen (note: pellets were split into two tubes to allow for geranylgeranyl and acetyl-CoA measurement from the same samples). For mass spectrometry analysis, samples were brought to room temperature and transferred to screw cap conical tubes. A modified Bligh-Dyer extraction using equal parts H_2O, methanol and dichloromethane (DCM) was used to lyse cells and solubilize lipids. The organic phase (containing lipids) was transferred to a new tube and dried under nitrogen. To eliminate the abundant glycerolipids and glycerophospholipids, samples were hydrolyzed with 1 ml 0.5 M KOH in methanol for 1 h at 80 °C. Samples were cooled to room temperature, and 1 ml of both H_2O and DCM were added to isolate geranylgeranyl. The organic layer (bottom) was transferred to a 1 ml glass insert inside a microcentrifuge tube. Samples were centrifuged at 8,000 rpm for 5 min to pellet insoluble material, and the supernatant was transferred to a new glass insert and dried under nitrogen. The samples were resuspended in 450 µl 90% methanol, and 45 µl of each sample was injected into a Shimadzu LC-20XR HPLC and analysed on an SCIEX API 5000 mass spectrometer in positive electrospray mode. A 12 min liquid chromatography method was used with a binary gradient, where mobile phase A contained 90% methanol with 5 mM NH4OAc and phase B contained methanol with 5 mM NH4OAc. The flow rate was 0.3 ml min^{-1}. At the time of injection, B was set to 70% and reduced to 25% over 5 min. At 5.1 min, B was set to 0% and held for 3 min. At 8.1 min, B was returned to 70% for a 4 min equilibration. Geranylgeranyl was resolved using a Phenomenex Kinetex C18 column (100 × 3.0 mm, 1.7 µm particle size) held at 40 °C. Multiple reaction monitoring was optimized for the ammonium adduct, with a mass pair of 273.3 and 81.2 Da. Geranylgeranyl eluted at a retention time of 3.8 min. Total peak area reflecting the amount of geranylgeranyl in each sample was derived using Analyst Software (ver. 1.7, SCIEX).

Acetyl-CoA measurement

Acetyl-CoA levels were measured from the same samples used for geranylgeranyl measurement. In brief, day 1 adult CF512 worm pellets were aliquoted into 1.5 ml Eppendorf tubes and flash frozen in liquid nitrogen. For acetyl-CoA measurement, samples were thawed on ice, followed by homogenization with glass/zirconia beads in non-native lysis buffer (0.5% sodium dodecyl-sulfate, 1% Triton x-100, 1 mM EDTA, 50 mM Hepes, 150 mM NaCl) supplemented with EDTA-free protease inhibitor cocktail (Roche 11836170001). Protein concentration was determined using Pierce BCA protein assay (Thermo Fisher Scientific 23225), and concentrations were normalized across all samples. Samples were then deproteinized with 1 M perchloric acid (2 µl per mg of sample protein) and perchloric acid was precipitated with 3 M potassium bicarbonate (1 µl per 10 µl of sample volume). Sample pH within the range of 6–8 pH was verified using

litmus paper. Acetyl-CoA abundance was measured with the Acetyl-Coenzyme A Assay Kit (Sigma-Aldrich MAK039) according to the manufacturer's instructions. Fluorescence quantifications were performed at room temperature with a CLARIOstar plus fluorimeter (BMG LabTech).

Protein extraction and western blotting

All western blots were performed on late L4 larvae or day 1 adult worms. Animals were washed off the plates with M9 buffer, centrifuged at 1,000*g* for 30 s, and washed twice with M9 before being transferred to 1.5 ml Eppendorf tubes and rapidly flash frozen in liquid nitrogen. Frozen worm pellets were thawed on ice and worm extracts were generated by glass/zirconia bead disruption in non-denaturing lysis buffer (50 mM Hepes pH 7.4, 150 mM NaCl, 1mM EDTA, 1 % Triton, EDTA-free mini-protease inhibitor cocktail (Roche)). Crude lysates were subject to centrifugation at 8,000*g* at 4 °C for 5 min prior to protein determination with a BCA protein quantification kit (Thermo Scientific). Lysates were supplemented with 2× Laemmli sample buffer, boiled at 90 °C for 10 min, resolved by SDS–PAGE, transferred to 0.22 μm nitro-cellulose membranes, and subject to western blot analysis[25]. To best visualize GFP::Rab mobility shifts, SDS–PAGE gels (10%) were incubated overnight at 4 °C in pre-moistened paper towels. Electrophoresis was performed at a constant 80 V until the 37 kDa protein standard of the prestained protein ladder (EZ-RUN, Thermo Fisher Scientific) reached the bottom of the SDS–PAGE gels.

All antibodies were prepared in 5% BSA/PBST. Rabbit anti-α-tubulin (Abcam ab4074) and secondary goat anti-rabbit (LiCor 926–32211) antibodies were used at 1:10,000. Mouse anti-GFP antibody (Roche 1814460001 at 0.4 mg ml^{-1}) was used at 1:4,000 and secondary goat anti-mouse antibody (LiCor 926–68070) was used at 1:5,000. Western blots were imaged and quantified using Image Studio software (ver. 5.2, LI-COR Biosciences). The proportion of total GFP-tagged Rab signal was calculated for the prenylated and unprenylated forms of the proteins. Samples were run in triplicate and ratioed band intensities were averaged for each biological replicate. See Supplementary Fig. 1 for gel source data.

Statistical analysis

Statistical analyses, including Student's *t*-test, mixed-effects, Chi-squared and ANOVA with post-hoc multiple comparisons analysis, were conducted using Prism (ver. 9.0, GraphPad) and CLC Genomics Workbench (ver. 9.5, Qiagen Bioinformatics). For large worm populations, outliers were removed using the ROUT method ($Q = 1\%$) prior to analysis.

Reporting summary

Further information on research design is available in the Nature Research Reporting Summary linked to this paper.

Extended Data

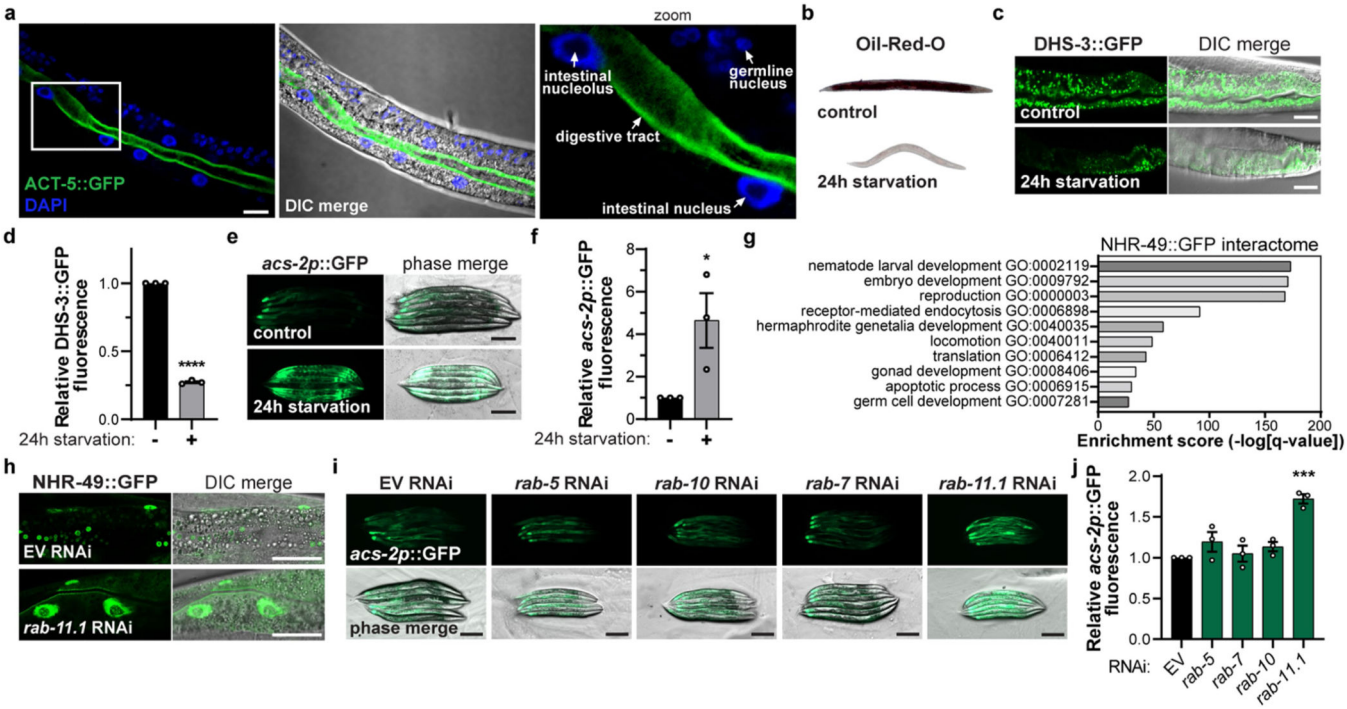

Extended Data Fig. 1 |. RAB-11.1-dependent cytosolic inactivation of NHR-49 in nutrient-rich conditions.

a, Representative micrograph of day 3 adult intestinal epithelia in transgenic worm expressing apical marker, ACT-5::GFP. Immunostaining for DAPI marks chromosomal DNA within nuclei. Reference Fig. 1b. Scale = 10 μm. $n = 4$ trials. **b**, Representative micrographs of Oil-Red-O-stained day 1 adult worms fed *ad libitum* (control) or starved for 24 h during late larval stages of development. $n = 3$ trials. **c,d**, Representative micrographs (**c**) and relative mean fluorescence by flow cytometry (**d**) of intestinal lipid droplet marker, DHS-3::GFP, in day 2 adults fed *ad libitum* (control, black) or starved for 24 h (grey). Scale = 25 μm. Mean ± SEM, ****$p < 0.0001$ by two-tailed unpaired t-test. $n = 3$ trials (circles). **e,f**, Fluorescence micrographs (**e**) and relative mean fluorescence by flow cytometry (**f**) of the *acs-2p*::GFP transcriptional reporter in day 1 adults fed *ad libitum* (control) or starved for 24 h. Scale = 200 μm. Mean ± SEM, ***$p < 0.0001$ by two-tailed unpaired t-test. $n = 3$ trials (circles). **g**, Gene Ontology (GO) term analysis from DAVID database. Plot displays the most over-represented biological processes (based on FDR) from proteins enriched by NHR-49::GFP co-immunoprecipitation and detected by liquid chromatography tandem mass spectrometry (LC-MS/MS). **h**, Representative confocal micrographs of NHR-49::GFP localization in day 1 adult intestinal epithelia in empty vector, EV, control or *rab-11.1* RNAi conditions. Scale = 10 μm. **i,j**, Fluorescence micrographs (**i**) and relative mean fluorescence by flow cytometry (**j**) of the *acs-2p*::GFP reporter in L4 larvae on EV RNAi (black) or RNAi for the respective Rab GTPases (green). Scale = 200 μm. Mean ± SEM, ***$p = 0.0003$ by one-way ANOVA with Dunnett's multiple comparisons test. $n = 3$ trials (circles).

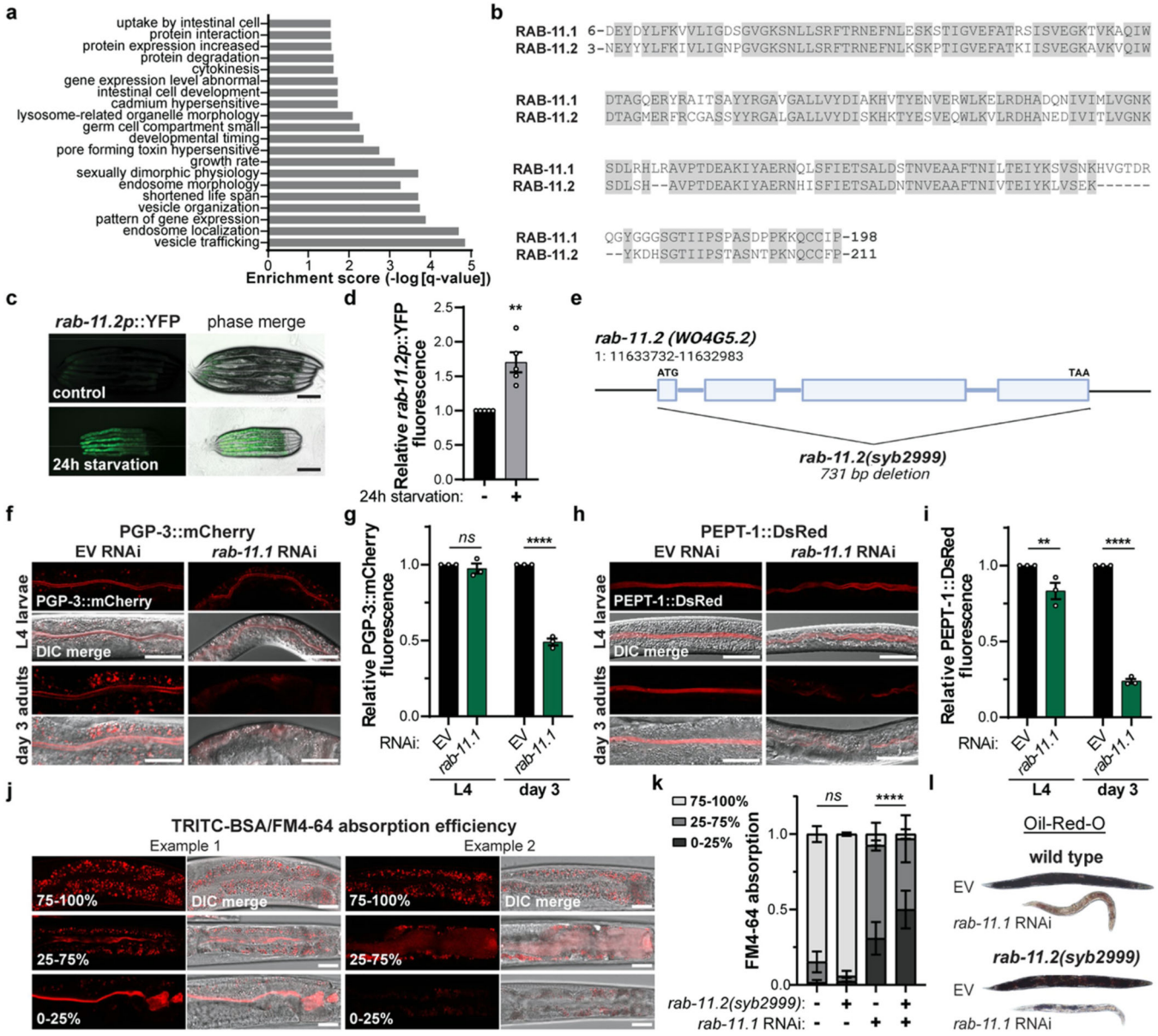

Extended Data Fig. 2 |. Adaptation to loss of RAB-11.1 through *rab-11.2* transcriptional induction.

a, Phenotype enrichment analysis (top 20) of genes differentially regulated ($p < 0.05$) upon *rab-11.1* RNAi. **b**, Amino acid sequence alignment for RAB-11.1 and RAB-11.2. **c,d**, Fluorescence micrographs (**c**) and relative mean fluorescence by flow cytometry (**d**) of the *rab-11.2p*::YFP transcriptional reporter in day 1 adults fed *ad libitum* (control, black) or starved for 24 h (grey). Scale = 200 μm. Mean ± SEM, ***$p < 0.0001$ by two-tailed unpaired t-test. $n = 5$ trials (circles). **e**, Schematic displays the *rab-11.2* gene and the respective *rab-11.2(syb2999)* mutation (731 base pair, bp, deletion). Blue box = exon, blue line = intron. **f-i**, Representative micrographs (**f,h**) and relative mean fluorescence by flow cytometry (**g,i**) of apical transporters, PGP-3::mCherry (**f,g**) and PEPT-1::DsRed (**h,i**), in L4 larvae and day 3 adults on EV (black) or *rab-11.1* (green) RNAi. Scale = 25 μm.

Mean ± SEM, ****$p < 0.0001$ (**g**) and **$p = 0.0058$, ****$p < 0.0001$ (**i**) by two-way ANOVA with Sidak's multiple comparisons test, *ns* = no significance. $n = 3$ trials for each timepoint (circles). **j**, Confocal micrographs of phenotypes representative of TRITC-BSA/FM4–64 absorption efficiency classification categories. Scale = 25 μm. **k**, Categorization of FM4–64 absorption efficiency following its dietary supplementation in day 2 adult wild type and *rab-11.2(syb2999)* worms on EV or *rab-11.1* RNAi. Shown is the relative ratio of animals which absorbed 0–25% (dark grey), 25–75% (medium grey), or 75–100% (light grey) of ingested FM4–64 into the intestinal epithelium. Mean ± SEM, ****$p < 0.0001$ by Chi-square test. $n = 64$ animals per condition over 2 trials. **l**, Representative micrographs of Oil-Red-O-stained day 5 adult wild type, WT, and *rab-11.2(syb2999)* worms on EV or *rab-11.1* RNAi. $n = 3$ trials.

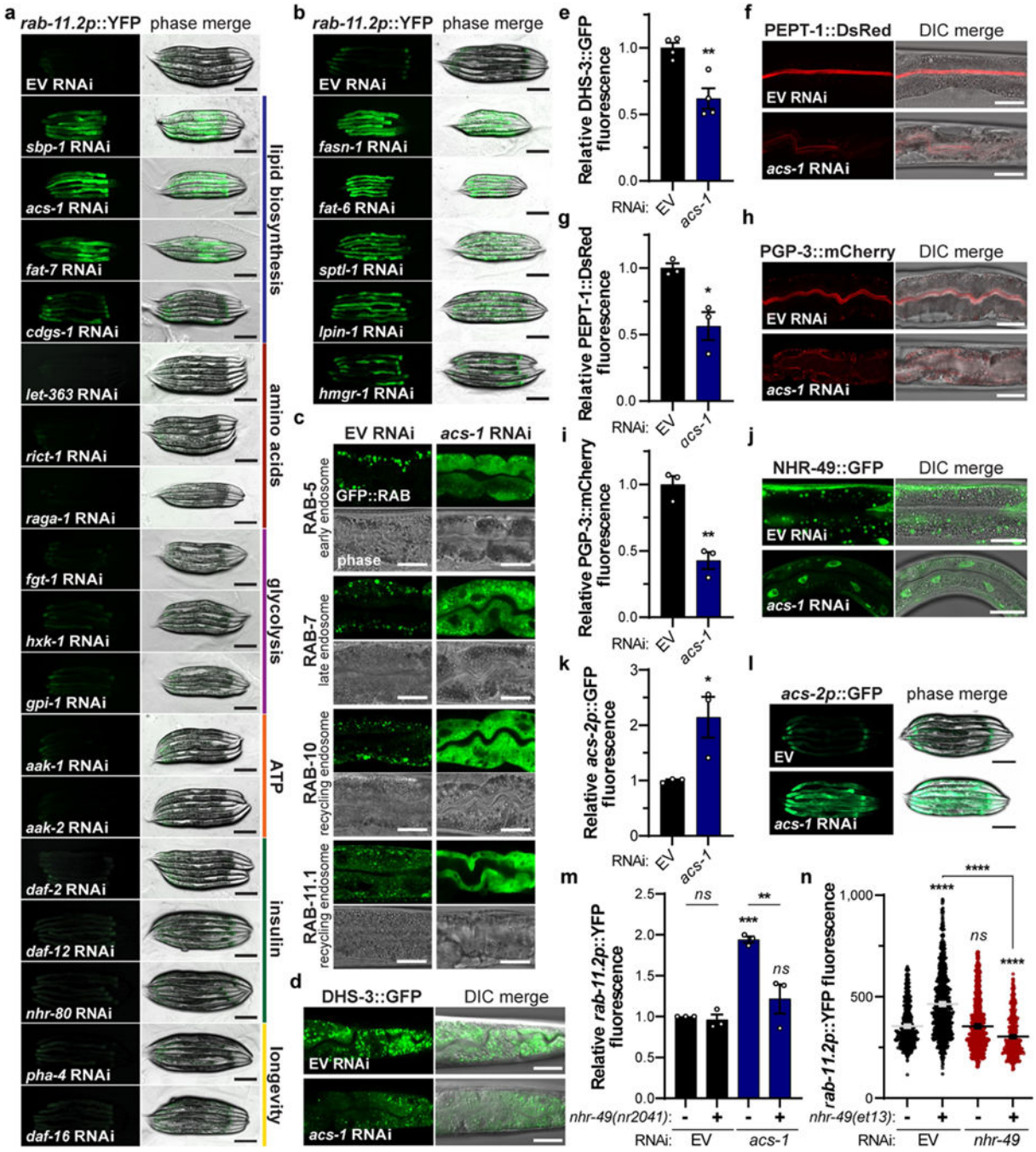

Extended Data Fig. 3 |. Lipid depletion activates *rab-11.2* through NHR-49.

a,b, Fluorescence micrographs of the *rab-11.2p*::YFP reporter in L4 larvae on empty vector, EV, control RNAi or RNAi for transcriptional and enzymatic effectors of various metabolic regulatory pathways (**a**) or critical enzymes in different lipid metabolism pathways (**b**). Reference Fig. 3a, b. Scale = 200 μm. **c**, Representative confocal micrographs of intestinal GFP::RAB transgene association with early, late, or recycling endocytic vesicles in day 2 adults on EV or *acs-1* RNAi. Scale = 25 μm. *n* = 3 trials. **d-i**, Representative micrographs (**d,f,h**) and relative mean fluorescence by flow cytometry (**e,g,i**) of lipid droplet marker,

DHS-3::GFP, (**d,e**) or apical transporters, PEPT-1::DsRed (**f,g**) and PGP-3::mCherry (**h,i**), in the intestines of day 3 adults on EV (black) or *acs-1* (blue) RNAi. Scale = 25 μm. Mean ± SEM, $^{**}p = 0.0045$ (**e**), $^{*}p = 0.0173$ (**g**), and $^{**}p = 0.0031$ (**i**) by two-tailed unpaired t-test. $n = 4$ trials in **e** and 3 trials in **g** and **I** (cirlces). **j**, Representative confocal micrographs of NHR-49::GFP localization in day 1 adults on EV or *acs-1* RNAi. Scale = 10 μm. **k,l**, Relative mean fluorescence by flow cytometry (**k**) and fluorescence micrographs (**l**) of the *acs-2p*::GFP reporter in day 1 adults on EV (black) or *acs-1* (blue) RNAi. Mean ± SEM, $^{*}p = 0.0360$ by two-tailed unpaired test. $n = 3$ trials (circles). Scale = 200 μm. **m**, Relative mean fluorescence by flow cytometry of the *rab-11.2p*::YFP reporter in wild type or *nhr-49(nr2041)* loss-of-function mutant day 1 adults on EV (black) or *acs-1* (blue) RNAi. Mean ± SEM, $^{**}p = 0.0032$, $^{***}p = 0.0006$, *ns* = no significance by two-way ANOVA with Tukey's multiple comparisons test. $n = 3$ trials (circles). **n**, Fluorescence of the *rab-11.2p*::YFP reporter by flow cytometry of wild type and *nhr-49(et13)* gain-of-function mutant day 1 adults on EV (black) or *nhr-49* (red) RNAi. Mean ± SEM, $^{****}p < 0.0001$ by one-way ANOVA with Dunnett's multiple comparisons test. From left to right, $n = 633$, 989, 499, and 553 animals (dots) over 3 trials.

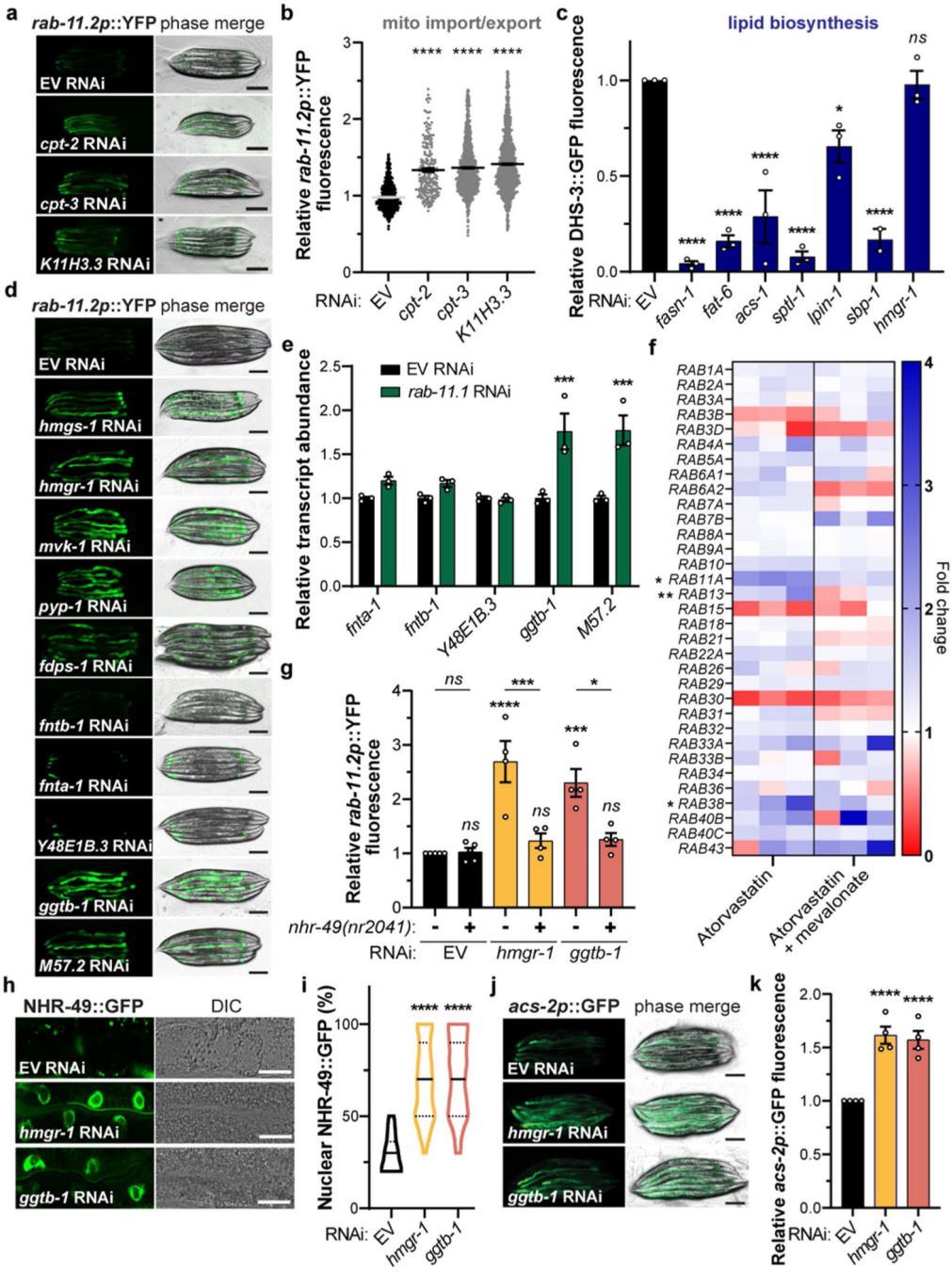

Extended Data Fig. 4 |. Inhibition of geranylgeranyl pyrophosphate synthesis or transfer to Rab GTPases is sufficient for pathway activation.

a,b, Fluorescence micrographs (**a**) and relative fluorescence by flow cytometry (**b**) of the *rab-11.2p*::YFP transcriptional reporter in day 1 adults on empty vector, EV, RNAi (black) or RNAi for enzymes involved in mitochondrial acyl-CoA import (*cpt-2/cpt-3*) and citrate export (*K11H3.3*) (grey). Scale = 200 μm. Mean ± SEM, ****$p < 0.0001$ by one-way ANOVA with Dunnett's multiple comparisons test. $n = 999$ (EV), 211 (*cpt-2*), 1399 (*cpt-3*) and 1546 (*K11H3.3*) animals (dots) across 3 trials. **c**, Relative mean DHS-3::GFP

fluorescence by flow cytometry of day 3 adults on EV RNAi (black) or RNAi for enzymes in different lipid metabolism pathways (blue). Reference Fig. 3a, b. Mean ± SEM, **p* = 0.0143, *****p* < 0.0001 by one-way ANOVA with Dunnett's multiple comparisons test, *ns* = no significance. *n* = 3 trials (circles). **d**, Fluorescence micrographs of the *rab-11.2p*::YFP reporter in day 1 adults on EV RNAi or RNAi for enzymes involved in prenol lipid synthesis and transfer to small G proteins. Reference Fig. 4a, b. Scale = 200 μm. **e**, Relative fold change in transcript abundance of the farnesyl and geranylgeranyl transferase holoenzyme subunits involved in small G protein prenylation upon *rab-11.1* RNAi. Reads per kilobase million, RPKM, standardized relative to EV RNAi control. Mean ± SEM, ****p* = 0.0005 and 0.0004 by two-way ANOVA with Sidak's multiple comparisons test. *n* = 3 biological replicates (circles). **f**, Heatmap displays the fold change in transcript abundance of Rab GTPases in primary human microvascular endothelial cells treated with either atorvastatin or atorvastatin + mevalonate in relation to vehicle (DMSO) control. Scale corresponds to relative fold change. Data were analyzed by two-way ANOVA with Tukey's multiple comparisons test, **p* = 0.0169 for *RAB11A*, **p* = 0.0450 for *RAB38*, and ***p* = 0.0078 for *RAB13* for transcripts differentially regulated by atorvastatin treatment in a mevalonate-dependent fashion. Reference Supplementary Table 1 for summary of statistics. *n* = 3 replicates. **g**, Relative mean fluorescence by flow cytometry of the *rab-11.2p*::YFP reporter in wild type or *nhr-49(nr2041)* day 1 adults on EV (black), *hmgr-1* (orange), or *ggtb-1* (red) RNAi. Reference Fig. 4c. Mean ± SEM, **p* = 0.0125, ****p* = 0.0004 and 0.0009, *****p* < 0.0001 by two-way ANOVA with Tukey's multiple comparisons test. *n* = 5 trials for EV and 4 trials for *hmgr-1* and *ggtb-1* RNAi (circles). **h,i**, Representative micrographs of NHR-49::GFP localization (**h**) and percent of intestinal epithelia with nuclear-localized NHR-49::GFP (**i**) in L4 larvae on EV (black), *hmgr-1* (orange), or *ggtb-1* (red) RNAi. Scale = 25 μm. Median with quartiles, *****p* < 0.0001 by one-way ANOVA with Tukey's multiple comparisons test. *n* = 50 animals per condition over 3 trials. **j,k**, Fluorescence micrographs (**j**) and relative mean fluorescence by flow cytometry (**k**) of the *acs-2p*::GFP reporter in day 1 adults on EV (black), *hmgr-1* (orange), or *ggtb-1* (red) RNAi. Scale = 200 μm. Mean ± SEM, *****p* < 0.0001 by one-way ANOVA with Tukey's multiple comparisons test. *n* = 4 trials (circles).

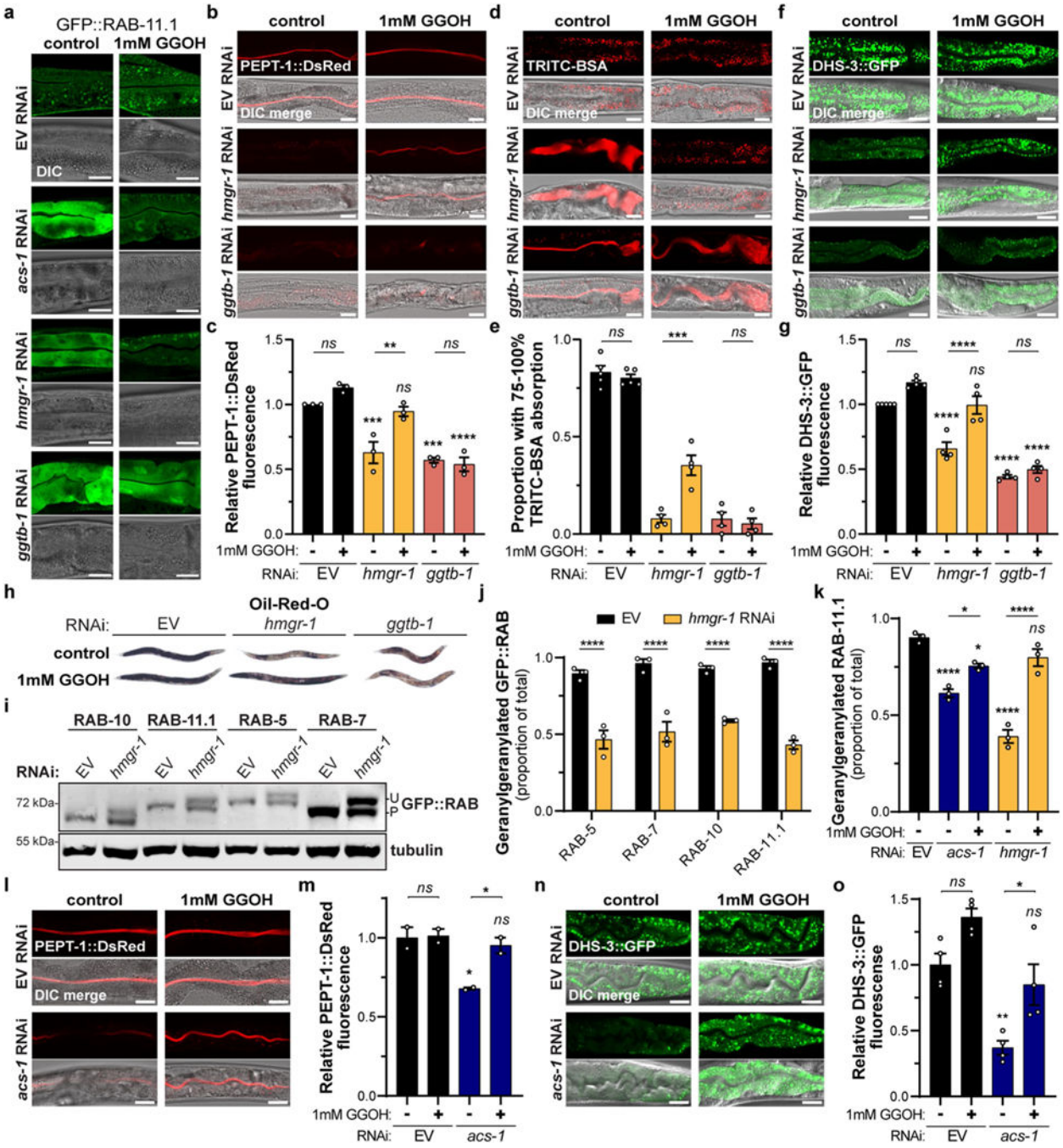

Extended Data Fig. 5 |. Ectopic geranylgeraniol supplementation restores vesicular trafficking and absorptive defects in a GGTB-1-dependent manner.

a, Representative micrographs of intestinal GFP::RAB-11.1 localization in day 2 adults on empty vector, EV, *acs-1, hmgr-1*, or *ggtb-1* RNAi ± 1mM GGOH. Scale = 25 μm. $n = 3$ trials. b,c, Representative micrographs (**b**) and relative mean fluorescence by flow cytometry (**c**) of PEPT-1::DsRed expression in day 4 adults on EV (black), *hmgr-1* (orange), or *ggtb-1* (red) RNAi ± 1mM GGOH. Scale = 25 μm. Mean ± SEM, $^{**}p = 0.0029$, $^{***}p = 0.0008$ and 0.0002, $^{****}p < 0.0001$ by two-way ANOVA with Tukey's multiple comparisons test,

ns = no significance. *n* = 3 trials (circles). **d,e,** TRITC-BSA absorption into the intestinal epithelium following its dietary supplementation in day 3 adults ultured at 25 °C on EV (black), *hmgr-1* (orange), or *ggtb-1* (red) RNAi ± 1mM GGOH. Representative micrographs (d) and proportion which absorbed 75–100% TRITC-BSA (**e**). Scale = 25 μm. Mean ± SEM, ****$p < 0.0001$ by two-way ANOVA with Tukey's multiple comparisons test. *n* = 5 trials for EV and 4 trials for *hmgr-1* and *ggtb-1* RNAi (circles). **f,g,** Representative micrographs (**f**) and relative mean fluorescence by flow cytometry (**g**) of DHS-3::GFP in day 3 adults on EV (black), *hmgr-1* (orange), or *ggtb-1* (red) RNAi ± 1mM GGOH. Scale = 25 μm. Mean ± SEM, ****$p < 0.0001$ by two-way ANOVA with Tukey's multiple comparisons test. *n* = 5 trials for EV and 4 trials for *hmgr-1* and *ggtb-1* RNAi (circles). **h**, Representative micrographs of Oil-Red-O-stained day 5 adults cultured at 25 °C on EV, *hmgr-1*, or *ggtb-1* RNAi ± 1mM GGOH. *n* = 3 trials. **i,j**, Western blot analysis of GFP::RAB transgene prenylation in EV (black) and *hmgr-1* (orange) RNAi conditions. Unprenylated ('U', top band) and prenylated ('P', bottom band) GFP::RABs with tubulin loading control (**i**) and proportion of total GFP::RAB signal in prenylated form (**j**). For gel source data, see Supplementary Fig. 1. Mean ± SEM, ****$p < 0.0001$ by two-way ANOVA with idak's multiple comparisons test. *n* = 3 trials (circles). **k**, Quantification of geranylgeranylated GFP::RAB-11.1 band intensity relative to total GFP::RAB-11.1 signal from western blot analysis of GFP::RAB-11.1 mobility in EV (black), *acs-1* (blue), and *hmgr-1* (orange) RNAi conditions ± 1mM GGOH. Reference Fig. 4e. Mean ± SEM, *$p = 0.0133$, ***$p = 0.0001$, ****$p < 0.0001$ by one-way ANOVA with Dunnett's multiple comparisons test. *n* = 3 trials (circles). **l,m**, Representative micrographs (**l**) and relative mean fluorescence by flow cytometry (**m**) of PEPT-1::DsRed in day 4 adults on EV (black) or *acs-1* (blue) RNAi ± 1mM GGOH. Scale = 25 μm. Mean ± SEM *$p = 0.0283$ and 0.0489 by two-way ANOVA with Tukey's multiple comparisons test. *n* = 2 trials (circles). **n,o**, Representative micrographs (**n**) and relative mean fluorescence by flow cytometry (**o**) of DHS-3::GFP in day 3 adults on EV (black) or *acs-1* (blue) RNAi ± 1mM GGOH. Scale = 25 μm. Mean ± SEM, *$p = 0.0217$, **$p = 0.0033$ by two-way ANOVA with Tukey's multiple comparisons test. *n* = 4 trials (circles).

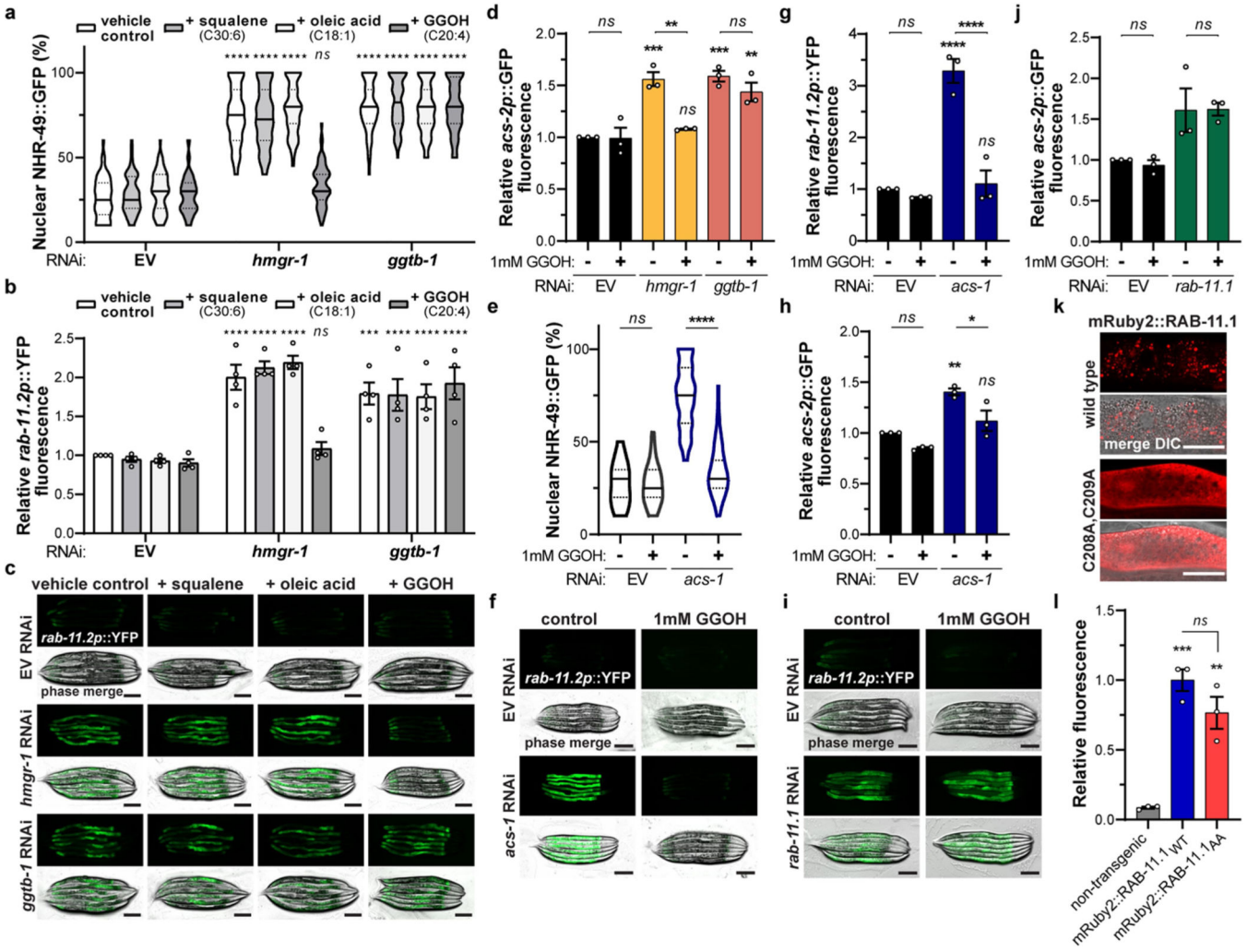

Extended Data Fig. 6 |. Geranylgeranyl availability and conjugation to RAB-11.1 are required for NHR-49 cytosolic inactivation.

a, Percent of intestinal epithelia with nuclear-localized NHR-49::GFP in day 1 adults on empty vector, EV, *hmgr-1*, or *ggtb-1* RNAi supplemented with vehicle control (white) or 1mM squalene (grey), oleic acid (light grey), or geranylgeraniol (GGOH) (dark grey). Median with quartiles, ****$p < 0.0001$ by two-way ANOVA with Tukey's multiple comparisons test, *ns* = no significance. $n = 90$ animals per condition over 3 trials. **b,c**, Relative mean fluorescence by flow cytometry (**b**) and fluorescence micrographs (**c**) of the *rab-11.2p*::YFP reporter in L4 larvae on EV, *hmgr-1*, or *ggtb-1* RNAi supplemented with vehicle control (white) or 1mM squalene (grey), oleic acid (light grey), or GGOH (dark grey). Mean ± SEM, ****$p < 0.0001$ by two-way ANOVA with Tukey's multiple comparisons test. $n = 4$ trials (circles). Scale= 200 μm. **d**, Relative mean fluorescence by flow cytometry of the *acs- 2p*::GFP reporter in day 1 adults on EV (black), *hmgr-1* (orange), or *ggtb-1* (red) RNAi ± 1mM GGOH. Mean ± SEM, **$p = 0.0023$, 0.0050 and ***$p = 0.006$, 0.004 by two-way ANOVA with Tukey's multiple comparisons test. $n = 3$ trials (circles). **e**, Percent of intestinal epithelia with nuclear-localized NHR-49::GFP in day 1 adults on EV (black) or *acs-1* (blue) RNAi ± 1mM GGOH. Median with quartiles, ****p

< 0.0001 by two-way ANOVA with Tukey's multiple comparisons test. $n = 55$ animals per condition over 3 trials. **f-h**, Fluorescence micrographs (**f**) and relative mean fluorescence by flow cytometry (**g,h**) of the *rab-11.2p*::YFP (**f,g**) or *acs-2p*::GFP (**h**) reporters in day 1 adults on EV (black) or *acs-1* (blue) RNAi ± 1mM GGOH. Scale = 200 μm. Mean ± SEM, ****$p < 0.0001$ (**g**) and *$p = 0.0222$, **$p = 0.0030$ (**h**) by two-way ANOVA with Tukey's multiple comparisons test. $n = 3$ trials (circles). **i**, Fluorescence micrographs of the *rab-11.2p*::YFP reporter in L4 larvae on EV (black) or *rab-11.1* (green) RNAi ± 1mM GGOH. Scale = 200 μm. **j**, Relative mean fluorescence by flow cytometry of the *acs-2p*::GFP reporter in L4 larvae on EV (black) or *rab-11.1* (green) RNAi ± 1mM GGOH. Mean ± SEM, $p = 0.0014$, *ns* = no significance by two-way ANOVA with Tukey's multiple comparisons test. $n = 3$ trials (circles). **k**, Representative confocal micrographs of mRuby2::RAB-11.1WT (wild type, top) or mRuby2::RAB-11.1C208A,C209A (prenylation motif mutant, bottom) localization within day 1 adult intestinal epithelia. Scale = 25 μm. **l**, Relative mean fluorescence by flow cytometry of day 1 adult transgenic worms expressing mRuby2::RAB-11.1WT (red) or mRuby2::RAB-11.1C208A,C209A (blue) compared to non-transgenic control (grey). Mean ± SEM, **$p = 0.0024$, ***$p = 0.0005$ by one-way ANOVA with Tukey's multiple comparisons test. $n = 3$ trials (circles).

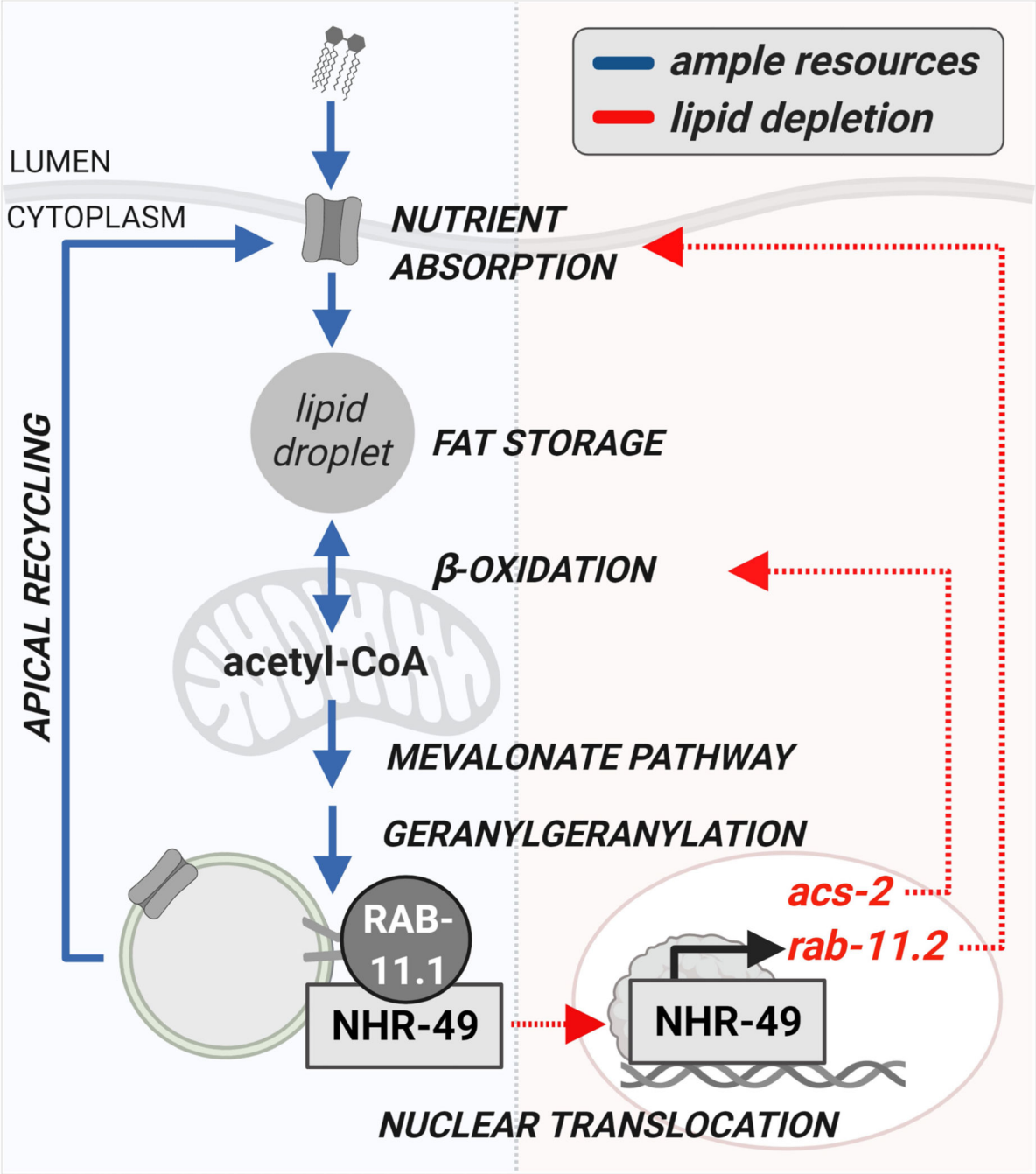

Extended Data Fig. 7 |. Model of intracellular lipid surveillance pathway.
In conditions of ample resources (blue, left), NHR-49 is sequestered to endocytic vesicles in a RAB-11.1 geranylgeranylation-dependent manner. Upon lipid depletion (red, right), NHR-49 translocates to the nucleus and activates a transcriptional program to restore lipid homeostasis and nutrient absorption.

Extended Data Table 1 |

Enrichment status of endocytosis (KEGG pathway cel04144) proteins in NHR-49::GFP immunoprecipitation (IP)/LC-MS/MS dataset (relative to non-transgenic control)

Protein	Enriched in NHR-49::GFP IP	Protein	Enriched in NHR-49::GFP IP	Protein	Enriched in NHR-49::GFP IP
AGEF-1	yes	EPN-1	yes	RME-1	no
ALX-1	yes	ERP-1	no	SLI-1	no
AMPH-1	no	F07F6.4	yes	SNX-1	yes
A PA-2	yes	F11F1.1	no	SNX-3	yes
APB-1	yes	F44E5.4	no	SNX-6	yes
APS-2	no	F44E5.5	no	SPG-20	no
ARF-1.2	yes	GBF-1	yes	SRC-1	yes
ARF-6	yes	GRK-1	yes	STAM-1	no
ARR-1	no	GRK-2	no	T05E7.3	no
ARX-3	no	GRP-1	no	T24B8.2	yes
ARX-4	yes	HGRS-1	yes	TSG-101	yes
ARX-5	yes	HSP-1	yes	UNC-57	yes
ARX-6	yes	HSP-70	no	UNC-116	yes
ARX-7	yes	ISTR-1	yes	USP-50	no
BRIS-1	yes	K02B12.7	no	VPS-2	yes
C01A2.4	yes	LET-23	no	VPS-4	yes
C46H11.3	no	MVB-12	yes	VPS-20	yes
CAP-1	yes	PAR-3	no	VPS-22	no
CAP-2	yes	PAR-6	yes	VPS-24	yes
CAV-1	yes	PKC-3	yes	VPS-25	yes
CAV-2	yes	PLD-1	yes	VPS-26	no
C DC-42	yes	PPK-1	yes	VPS-29	yes
CHC-1	yes	PPK-3	no	VPS-32.1	yes
CNT-1	no	R12C12.5	no	VPS-32.2	no
CNT-2	yes	RAB-5	yes	VPS-35	yes
CRP-1	no	RAB-7	yes	VPS-36	no
DDL-1	no	RAB-8	yes	VPS-37	no
DDL-2	no	RAB-10	yes	VPS-60	no
DID-2	yes	RAB-11.1	yes	W09D10.1	no
DPY-23	yes	RAB-11.2	no	WSP-1	no
DYN-1	yes	RAB-35	yes	WWP-1	yes
EEA-1	no	RABS-5	no	Y53F4B.21	no
EFA-6	no	RFIP-1	no	Y92H12A.2	no
EHS-1	yes	RHO-1	yes	**59 yes/101 total**	

Supplementary Material

Refer to Web version on PubMed Central for supplementary material.

Acknowledgements

We thank A. Ghazi for the NHR-49::GFP (AGP33a) worm strain; M. Zerial for the PEPT-1::DsRed worm strain (MZE1); SunyBiotech for generation and validation of the *rab-11.2(syb2999)* (PHX2999) and GFP::RAB-11.1 (PHX4435) worm strains; the Caenorhabditis Genetics Center (CGC) for worm strains; A. Lemoff and the UT Southwestern Medical Center Mass Spectrometry Core for LC-MS/MS support; and M. Buszczak and M. Douglas for critical review of the manuscript. We acknowledge S. Schmid, K. Dean, R. Debose-Boyd, D. Russell and J. Goldstein for critical discussions. This work has been funded by the Clayton Foundation for Research, the Welch Foundation (I-2061-20210327), the NIH (R00AG042495, R01AG061338, and R56AG070167) and the Cancer Prevention Research Institute of Texas (RR150089). Schematics were created with BioRender.com.

Data availability

All data generated and analysed during this study are included in this article and its Supplementary Information and are also available from the authors upon request. Transcriptomic data files that support the findings of this study in *C. elegans* have been deposited in the NCBI Gene Expression Omnibus (GEO) under accession GSE189106. Source data are provided with this paper.

References

1. Morton GJ, Cummings DE, Baskin DG, Barsh GS & Schwartz MW Central nervous system control of food intake and body weight. Nature 443, 289–295 (2006). [PubMed: 16988703]
2. Caspi L, Wang PY & Lam TK A balance of lipid-sensing mechanisms in the brain and liver. Cell Metab. 6, 99–104 (2007). [PubMed: 17681145]
3. Ashrafi K. et al. Genome-wide RNAi analysis of *Caenorhabditis elegans* fat regulatory genes. Nature 421, 268–272 (2003). [PubMed: 12529643]
4. Van Gilst MR, Hadjivassiliou H. & Yamamoto KR A *Caenorhabditis elegans* nutrient response system partially dependent on nuclear receptor NHR-49. Proc. Natl Acad. Sci. USA 102, 13496–13501 (2005). [PubMed: 16157872]
5. Ratnappan R. et al. Germline signals deploy NHR-49 to modulate fatty-acid β-oxidation and desaturation in somatic tissues of *C. elegans*. PLoS Genet. 10, e1004829 (2014).
6. Chawla A, Repa JJ, Evans RM & Mangelsdorf DJ Nuclear receptors and lipid physiology: opening the X-files. Science 294, 1866–1870 (2001). [PubMed: 11729302]
7. Levin ER & Hammes SR Nuclear receptors outside the nucleus: extranuclear signalling by steroid receptors. Nat. Rev. Mol. Cell Biol. 17, 783–797 (2016). [PubMed: 27729652]
8. Burkewitz K. et al. Neuronal CRTC-1 governs systemic mitochondrial metabolism and lifespan via a catecholamine signal. Cell 160, 842–855 (2015). [PubMed: 25723162]
9. Stenmark H. Rab GTPases as coordinators of vesicle traffic. Nat. Rev. Mol. Cell Biol. 10, 513–525 (2009). [PubMed: 19603039]
10. Palm W. & Thompson CB Nutrient acquisition strategies of mammalian cells. Nature 546, 234–242 (2017). [PubMed: 28593971]
11. Eaton S. Control of mitochondrial beta-oxidation flux. Prog. Lipid Res. 41, 197–239 (2002). [PubMed: 11814524]
12. Rambold AS, Cohen S. & Lippincott-Schwartz J. Fatty acid trafficking in starved cells:regulation by lipid droplet lipolysis, autophagy, and mitochondrial fusion dynamics. Dev. Cell 32, 678–692 (2015). [PubMed: 25752962]
13. Welz T, Wellbourne-Wood J. & Kerkhoff E. Orchestration of cell surface proteins by Rab11. Trends Cell Biol. 24, 407–415 (2014). [PubMed: 24675420]
14. Grevengoed TJ, Klett EL & Coleman RA Acyl-CoA metabolism and partitioning. Annu. Rev. Nutr. 34, 1–30 (2014). [PubMed: 24819326]
15. Lee K, Goh GY, Wong MA, Klassen TL & Taubert S. Gain-of-function alleles in *Caenorhabditis elegans* nuclear hormone receptor nhr-49 are functionally distinct. PLoS ONE 11, e0162708 (2016).

16. Judge A. & Dodd MS Metabolism. Essays Biochem. 64, 607–647 (2020). [PubMed: 32830223]
17. Pietrocola F, Galluzzi L, Bravo-San Pedro JM, Madeo F. & Kroemer G. Acetyl coenzyme A: a central metabolite and second messenger. Cell Metab. 21, 805–821 (2015). [PubMed: 26039447]
18. Goldstein JL & Brown MS Regulation of the mevalonate pathway. Nature 343, 425–430 (1990). [PubMed: 1967820]
19. Seabra MC, Brown MS, Slaughter CA, Sudhof TC & Goldstein JL Purification of component A of Rab geranylgeranyl transferase: possible identity with the choroideremia gene product. Cell 70, 1049–1057 (1992). [PubMed: 1525821]
20. Zhang FL & Casey PJ Protein prenylation: molecular mechanisms and functional consequences. Annu. Rev. Biochem. 65, 241–269 (1996). [PubMed: 8811180]
21. Rauthan M. & Pilon M. The mevalonate pathway in *C. elegans*. Lipids Health Dis. 10, 243 (2011). [PubMed: 22204706]
22. Gelb MH Protein prenylation, et cetera: signal transduction in two dimensions. Science 275, 1750–1751 (1997). [PubMed: 9122679]
23. Boerma M. et al. Comparative gene expression profiling in three primary human cell lines after treatment with a novel inhibitor of Rho kinase or atorvastatin. Blood Coag. Fibrin 19, 709–718 (2008).
24. Winter JF et al. *Caenorhabditis elegans* screen reveals role of PAR-5 in RAB-11-recycling endosome positioning and apicobasal cell polarity. Nat. Cell Biol. 14, 666–676 (2012). [PubMed: 22634595]
25. Egge N. et al. Age-onset phosphorylation of a minor actin variant promotes intestinal barrier dysfunction. Dev. Cell 51, 587–601.e587 (2019). [PubMed: 31794717]
26. Egge N. et al. Trauma-induced regulation of VHP-1 modulates the cellular response to mechanical stress. Nat. Commun. 12, 1484 (2021). [PubMed: 33674585]
27. de Souza N, Vallier LG, Fares H. & Greenwald I. SEL-2, the *C. elegans* neurobeachin/LRBA homolog, is a negative regulator of lin-12/Notch activity and affects endosomal traffic in polarized epithelial cells. Development 134, 691–702 (2007). [PubMed: 17215302]
28. Huang DW, Sherman BT & Lempicki RA Systemic and integrative analysis of large gene lists using DAVID bioinformatics resources. Nat. Protoc. 4, 44–57 (2009). [PubMed: 19131956]
29. Huang DW, Sherman BT & Lempicki RA Bioinformatics enrichment tools: paths toward the comprehensive functional analysis of large gene lists. Nucleic Acids Res. 37, 1–13 (2009). [PubMed: 19033363]
30. Angeles-Albores D, Lee RYN, Chan J. & Sternberg PW Tissue enrichment analysis for *C. elegans* genomics. BMC Bioinf. 17, 366 (2016).

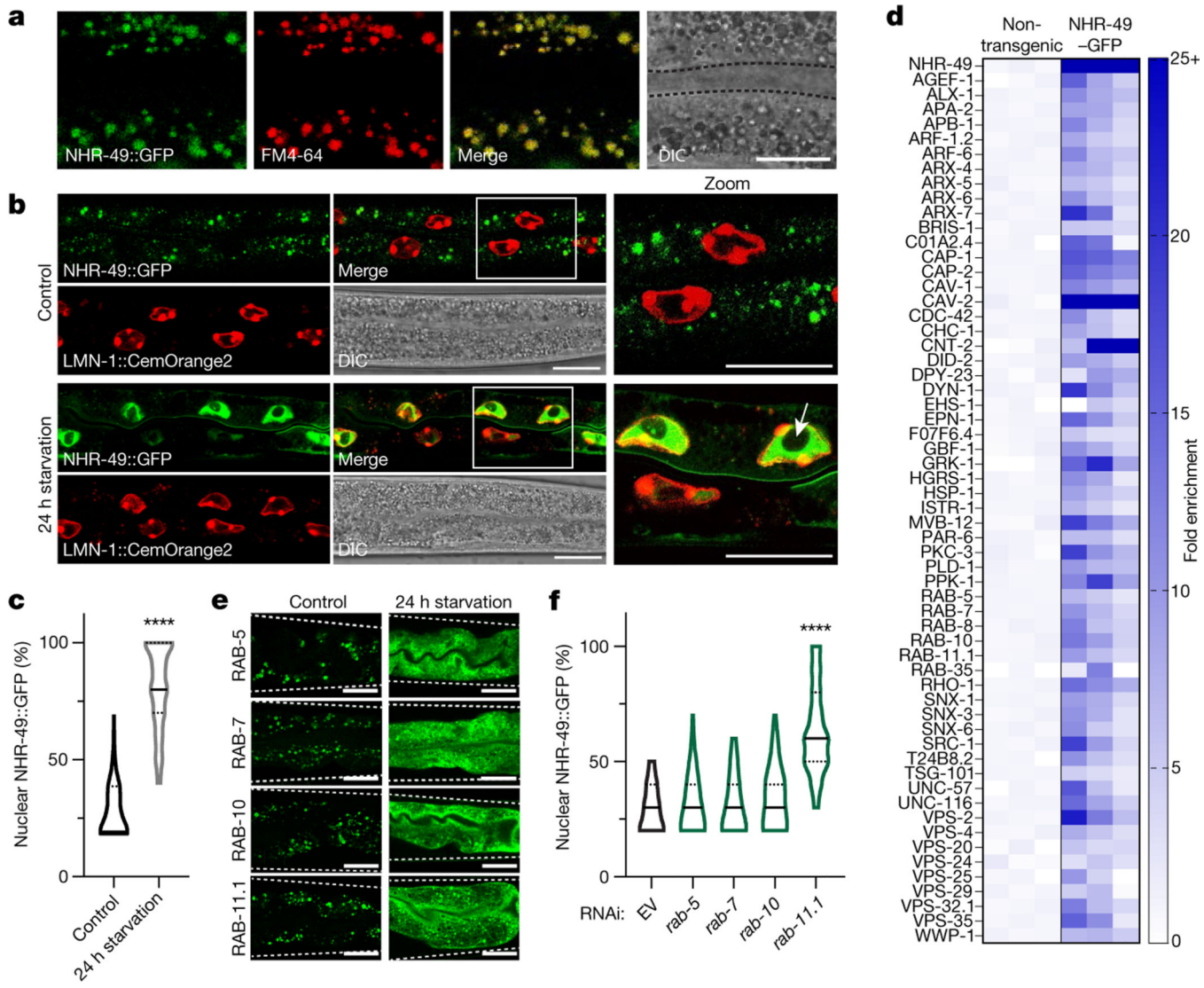

Fig. 1 |. Transcriptional inactivation of NHR-49 via cytosolic sequestration to endocytic transport vesicles.

a, **b**, Fluorescence micrographs showing NHR-49::GFP localization with the lipophilic dye FM4–64 (**a**) or nuclear lamin marker LMN-1::CemOrange2 (**b**) in day 1 adult intestinal epithelia. Dashed lines mark the digestive tract; the arrow marks nucleolus. Scale bars, 10 μm (**a**) and 25 μm (**b**). DIC, differential interference contrast image. **c**, Percentage of intestinal epithelial cells with nuclear-localized NHR-49::GFP in ad libitum-fed control or 24 h starved worms. Plots show median and quartiles. ****$P < 0.0001$ by two-tailed unpaired *t*-test. $n = 76$ (control) and 62 (starved) worms over 3 trials. **d**, Heat map of endocytosis-related proteins enriched in NHR-49::GFP immunoprecipitates relative to non-transgenic control (Extended Data Table 1). Scale corresponds to peptide enrichment. **e**, Fluorescence micrographs of different GFP::Rab fusion proteins in fed (control) or starvation conditions in day 2 adult intestinal epithelia. Dashed lines mark the worm exterior. Scale, 25 μm. $n = 3$ trials. **f**, Percentage of intestinal epithelial cells with nuclear-localized NHR-49::GFP in worms treated with empty vector (EV) or RNAi for the indicated Rab

GTPases. Plots show median and quartiles. ****$P < 0.0001$ by one-way ANOVA with Dunnett's test. $n = 70$ over 3 trials.

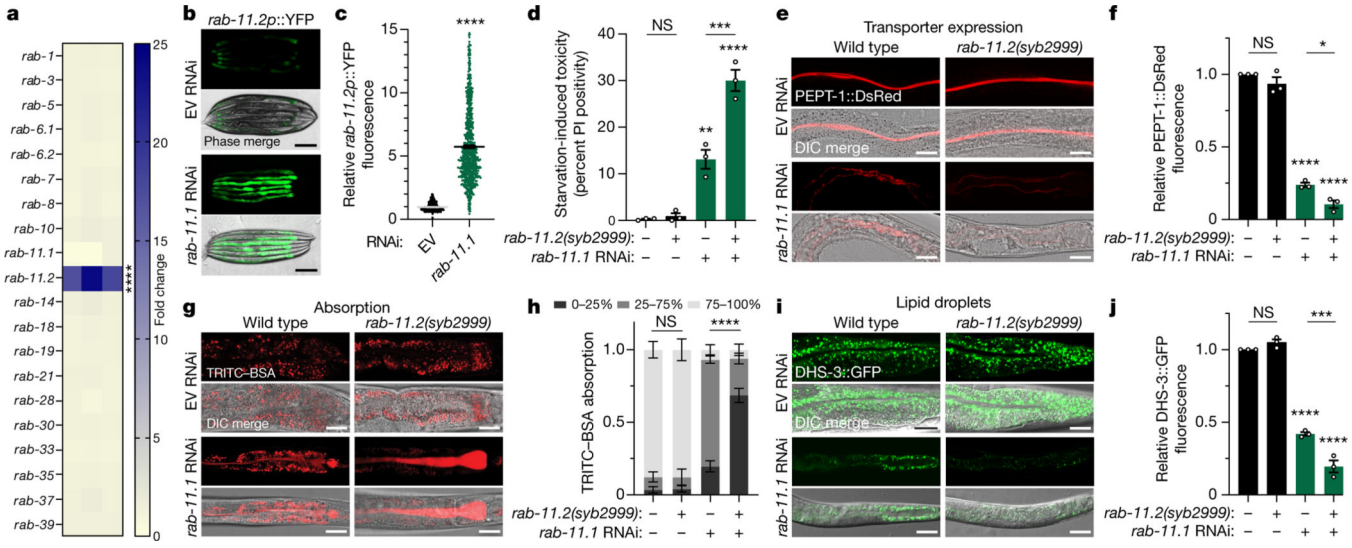

Fig. 2 |. Adaptation to loss of RAB-11.1 by *rab-11.2* activation.

a, Transcript abundance of Rab GTPases upon treatment with *rab-11.1* RNAi. Scale corresponds to relative fold change. ****$P < 0.0001$ by one-way ANOVA with Dunnett's test. **b**, **c**, Fluorescence micrographs (**b**) and relative fluorescence by flow cytometry (**c**) of the *rab-11.2p*::YFP transcriptional reporter in day 1 adults treated with empty vector or *rab-11.1* RNAi. Scale bars, 200 μm. Data are mean ± s.e.m. ****$P < 0.0001$ by two-tailed unpaired *t*-test. $n = 1{,}453$ (empty vector) and 800 (*rab-11.1*) over 4 trials. **d**, Percentage of day 1 adults with positive propidium iodide (PI) staining after starvation for 24 h in wild-type and *rab-11.2(syb2999)* mutant worms treated with empty vector (black) or *rab-11.1* (green) RNAi. Data are mean ± s.e.m. **$P = 0.0024$, ***$P = 0.0008$, ****$P < 0.0001$; two-way ANOVA with Sidak's test. $n = 3$ trials (circles). **e**, **f**, Confocal micrographs (**e**) and relative mean fluorescence by flow cytometry (**f**) of PEPT-1::DsRed expression in wild-type and *rab-11.2(syb2999)* day 4 adults treated with empty vector (black) or *rab-11.1* (green) RNAi. Scale bars, 25 μm. Data are mean ± s.e.m. *$P = 0.0336$, ****$P < 0.0001$; two-way ANOVA with Tukey's test. $n = 3$ trials (circles). **g**, **h**, Representative micrographs (**g**) and efficiency (**h**) of TRITC–BSA intestinal absorption in wild-type and *rab-11.2(syb2999)* day 2 adults treated with empty vector or *rab-11.1* RNAi. Scale bars, 25 μm. Categorization of TRITC–BSA absorption efficiency: 0–25% (dark grey), 25–75% (medium grey) and 75–100% (light grey) (Extended Data Fig. 2j). Data are mean ± s.e.m. ****$P < 0.0001$ by Chi-square test. $n = 105$ over 3 trials. **i**, **j**, Representative micrographs (**i**) and relative mean fluorescence by flow cytometry (**j**) of DHS-3::GFP expression in wild-type and *rab-11.2(syb2999)* day 3 adults treated with empty vector (black) or *rab-11.1* (green) RNAi. Scale bars, 25 μm. Data are mean ± s.e.m. ***$P = 0.0008$, ****$P < 0.0001$; two-way ANOVA with Tukey's test. $n = 3$ trials (circles). NS, not significant.

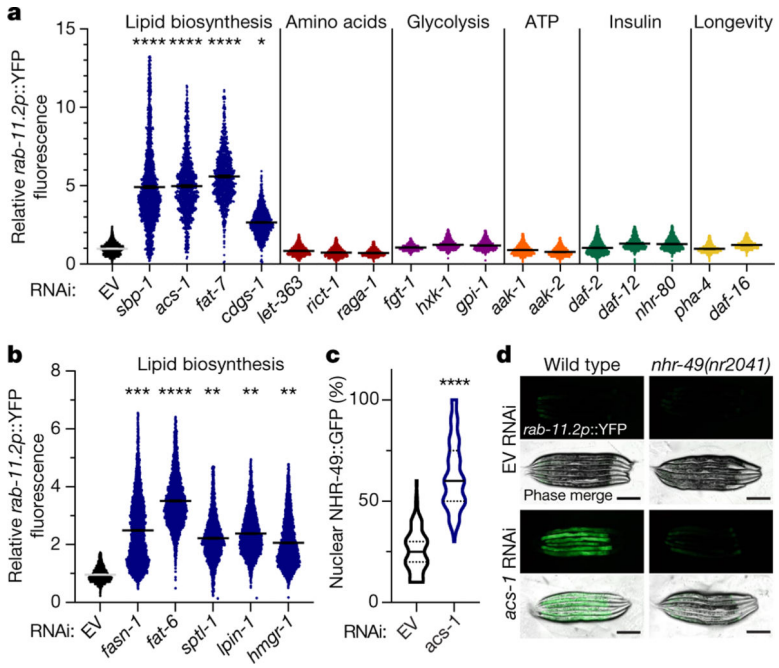

Fig. 3 |. Lipid depletion activates *rab-11.2* transcription through NHR-49.

a, **b**, Relative fluorescence of the *rab-11.2p*::YFP reporter by flow cytometry in day 1 adults on empty vector RNAi or RNAi for regulators of lipid biosynthesis, amino acid metabolism, glycolysis, ATP sensing, insulin signalling and longevity (**a**) or for enzymes involved in fatty acid synthesis (*fasn-1*), biosynthesis of unsaturated fatty acids (*fat-6*), sphingolipid metabolism (*sptl-1*), glycerophospholipid metabolism (*lpin-1*) or prenollipid synthesis (*hmgr-1*) (**b**). Data are mean ± s.e.m. **a**, *cdgs-1*: $*P = 0.0302$; $****P < 0.0001$. **b**, *fasn-1*: $***P = 0.0009$; *sptl-1*: $**P = 0.0062$; *lpin-1*: $**P = 0.0036$; *hmgr-1*: $**P = 0.0073$; $****P < 0.0001$). Analysis of relative mean fluorescence from each trial by one-way ANOVA with Dunnett's test. From left to right in **a**, $n = 12,099$, 2,403, 1,188, 969, 1,934, 4,903, 1,496, 1,433, 1,596, 1,632, 1,547, 2,954, 2,893, 2,516, 3,141, 3,473, 3,958 and 3,459 worms (dots) over 9 trials for empty vector and 3 trials for all other RNAi. From left to right in **b**, $n = 5,861$, 9,539, 5,055, 3,439, 5,094 and 6,238 worms (dots) over 3 trials. **c**, Percentage of intestinal epithelial cells with nuclear-localized NHR-49::GFP in day 1 adults on empty vector or *acs-1* RNAi. Data are median with quartiles. $****P < 0.0001$ by two-tailed unpaired *t*-test. $n = 94$ (empty vector) and 91 (*acs-1*) over 3 trials. **d**, Fluorescence micrographs of the *rab-11.2p*::YFP reporter in wild-type and *nhr-49(nr2041)* mutant L4 larvae on empty vector or *acs-1* RNAi. Scale bars, 200 μm.

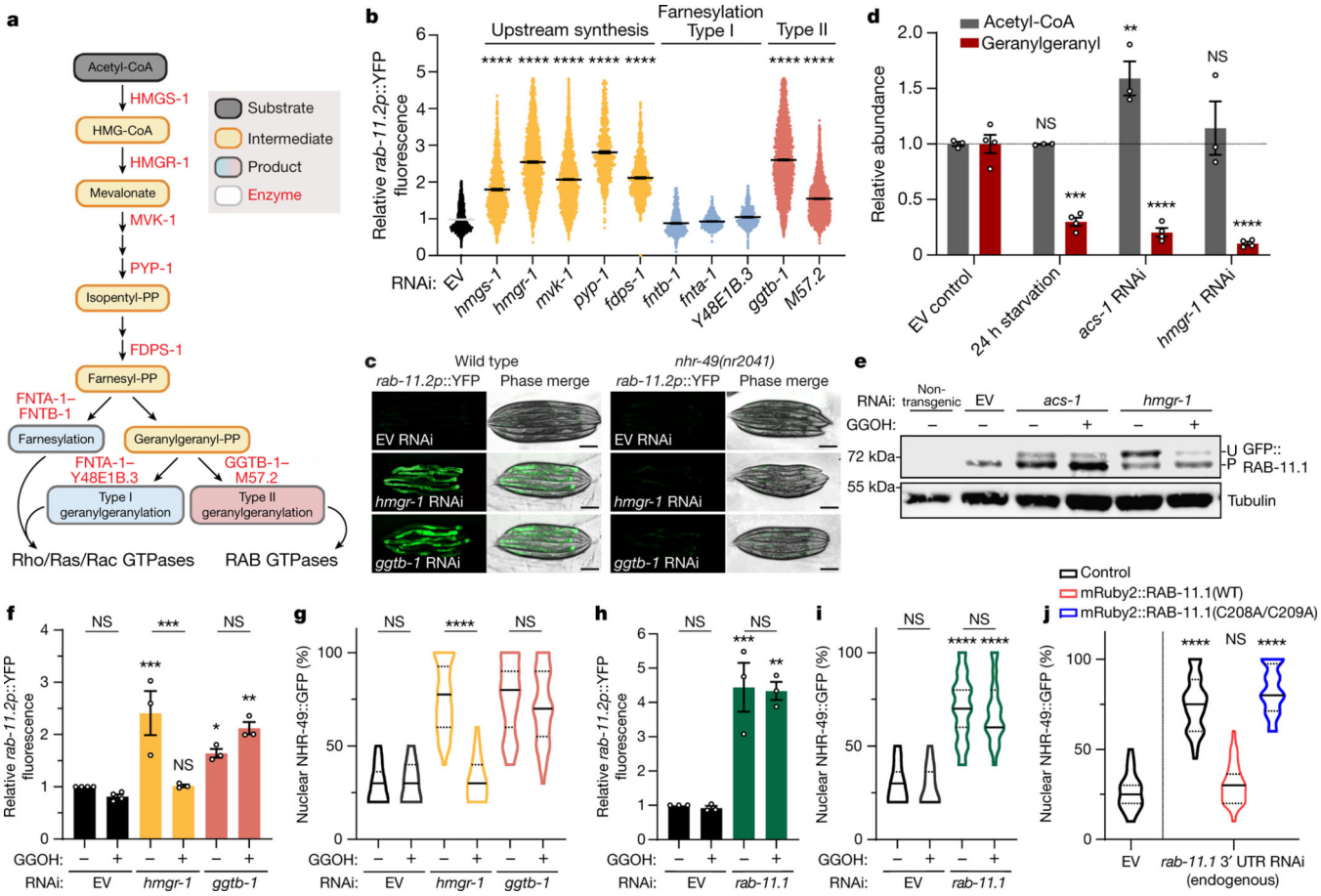

Fig. 4 |. Geranylgeranyl synthesis and conjugation to RAB-11.1 are required for NHR-49 cytosolic inactivation.

a, Schematic showing major metabolites and enzymes required for small G protein prenylation in *C. elegans*. FDPS-1, farnesyl diphosphate synthetase; FNTA-1, farnesyltransferase α-subunit; FNTB-1, farnesyltransferase β-subunit; HMGS-1, hydroxymethylglutaryl-CoA synthase; M57.2, geranylgeranyl transferase type II α-subunit; MVK-1, mevalonate kinase; PYP-1, inorganic pyrophosphatase 1; Y48E1B.3, geranylgeranyl transferase type I β-subunit. **b**, Relative *rab-11.2p*::YFP fluorescence with empty vector RNAi or RNAi for enzymes responsible for isopentyl pyrophosphate (PP) synthesis (orange), farnesyl and type I geranylgeranyl transfer (blue) or type II geranylgeranyl transfer (red). Data are mean ± s.e.m. ****$P < 0.0001$ by one-way ANOVA with Dunnett's test. $n > 482$ worms over 5 (empty vector) or 3 trials. **c**, *rab-11.2p*::YFP fluorescence in wild-type and *nhr-49(nr2041)* worms treated with the indicated RNAi. Scale bars, 200 μm. **d**, Relative acetyl-CoA and geranylgeranyl levels in day 1 adults. Data are mean ± s.e.m. **$P = 0.0031$, ***$P = 0.0003$, ****$P < 0.0001$; two-way ANOVA with Sidak's test. $n = 3$ (acetyl-CoA) and 4 (geranylgeranyl). **e**, Western blots of unprenylated (U) versus prenylated (P) GFP::RAB-11.1 with empty vector, *acs-1* or *hmgr-1* RNAi with or without 1 mM geranylgeraniol (GGOH). For gel source data, see Supplementary Fig. 1.f–h, Relative mean *rab-11.2p*::YFP fluorescence (**f**, **h**) and percentage of intestinal epithelial cells with nuclear-localized NHR-49::GFP (**g**, **i**) following treatment with empty vector and

hmgr-1 or *ggtb-1* RNAi (**f**, **g**) or *rab-11.1* RNAi (**h**, **i**) with or without GGOH. Data in **f**, **h** are mean ± s.e.m.; data in **g**, **i** are median with quartiles. **f**, **P* = 0.0320, ***P* = 0.0022, ****P* = 0.0002 (*hmgr-1* versus EV), 0.0005 (*hmgr-1* ± GGOH). **g**, **i**, *****P* < 0.0001. **h**, ***P* = 0.0012, ****P* = 0.0010. Two-way ANOVA with Tukey's test. *n* = 4 (empty vector) and 3 (*hmgr-1* and *ggtb-1*) trials in **f**, *n* = 3 in **h**, *n* = 50 over 3 trials in **g**, **i**. **j**, Percentage of nuclear-localized NHR-49::GFP in transgenic worms expressing NHR-49::GFP alone (control) or with intestinal expression of wild-type RAB-11.1 (mRuby2::RAB-11.1) or the prenylation mutant (mRuby2::RAB-11.1(C208A/C209A)) with empty vector or *rab-11.1* 3′ UTR RNAi. Data are median with quartiles. *****P* < 0.0001 by one-way ANOVA with Tukey's test. *n* = 50 over 3 trials.